Brucella EipB is a periplasmic β-spiral protein required for envelope stress resistance and infection

Julien Herrou[a,#,¶], Jonathan W. Willett[a,#], Aretha Fiebig[a], Daniel M. Czyż[b], Jason X. Cheng[c], Eveline Ultee[d], Ariane Briegel[d], Lance Bigelow[e], Gyorgy Babnigg[e], Youngchang Kim[e], and Sean Crosson[a*]

[a]Department of Biochemistry and Molecular Biology, University of Chicago, Chicago, IL, USA.
[b]Department of Microbiology and Cell Science, University of Florida, Gainesville, IL, USA
[c]Department of Pathology, The University of Chicago, Chicago, IL, USA
[d]Department of Biology, Universiteit Leiden, Leiden, Netherlands
[e]Biosciences Division, Argonne National Laboratory, Argonne, IL, USA

* To whom correspondence should be addressed, scrosson@uchicago.edu
[#] Contributed equally to this work
[¶] Current location: Laboratoire de Chimie Bactérienne, Institut de Microbiologie de la Méditerranée, CNRS, Marseille, France.

Summary
The Gram-negative cell envelope is a remarkably diverse structure with core components that include an inner membrane, an outer membrane, and a peptidoglycan layer in the periplasmic space between. We show that a conserved DUF1849-family protein, EipB, is secreted to the periplasmic space of *Brucella*, a monophyletic group of intracellular pathogens. In the periplasm, EipB folds into an unusual fourteen-stranded β-spiral structure that contains a conserved disulfide bond. EipB has structural features that resemble the LolA and LolB lipoprotein delivery system, though the overall topology and fold of EipB is distinct from LolA/LolB. Deletion of *eipB* results in defects in both cell envelope integrity *in vitro* and in maintenance of spleen colonization in a mouse model of *B. abortus* infection. Transposon disruption of *ttpA*, which encodes a periplasmic tetratricopeptide repeat (TPR) protein, is synthetically lethal with *eipB* deletion in *B. abortus*. *ttpA* is a known virulence determinant in *B. melitensis*, and our studies of *ttpA* deletion and overexpression strains provide evidence that *ttpA*, like *eipB*, contributes to cell envelope function in *Brucella*. We conclude that *eipB* and *ttpA* function in the *Brucella* periplasmic space to maintain cell envelope integrity and to facilitate survival in a mammalian host.

Importance
Brucella species cause brucellosis, a global zoonosis. A gene encoding a conserved uncharacterized protein, EipB, is present in all sequenced *Brucella* and several other genera in the class *Alphaproteobacteria*. To our knowledge, this study presents the first functional and structural characterization of a protein from the DUF1849 family, to which EipB belongs. EipB is secreted to the periplasm where it forms a spiral-like anti-parallel β structure. Deletion of *Brucella eipB* results in defects of the cell envelope and in reduced virulence in an animal model of disease. *eipB* genetically interacts with *ttpA*, which also encodes a periplasmic protein. We propose that EipB and TtpA function as part of a system required for cell envelope homeostasis in select *Alphaproteobacteria*.

Introduction

Brucella spp. are the causative agents of brucellosis, which afflicts wildlife and livestock on a global scale and can occur in humans through contact with infected animals or animal products (1, 2). These intracellular pathogens are members of the class *Alphaproteobacteria*, a group of Gram-negative species that exhibit tremendous diversity in metabolic capacity, cell morphology, and ecological niches (3). In their mammalian hosts, *Brucella* cells must contend with the host immune system (4) and adapt to stresses including oxidative assault from immune cells, acidic pH in the phagosomal compartment, and nutrient shifts during intracellular trafficking (5). Molecular components of the cell envelope play a key role in the ability of *Brucella* spp. to survive these stresses and to replicate in the intracellular niche (6, 7). As part of a systematic experimental survey of conserved *Alphaproteobacterial* protein domains of unknown function (DUFs), we recently described envelope integrity protein A (EipA). This periplasmic protein confers resistance to cell envelope stressors and determines *B. abortus* virulence in a mouse model of infection (8). In this study, we report a functional and structural analysis of envelope integrity protein B (EipB), a member of the uncharacterized gene family DUF1849.

DUF1849 (Pfam: PF08904) is almost entirely restricted to the *Alphaproteobacteria* (9). Within this taxonomic class, it is widespread among the *Rhizobiales*, *Rhodospirillales* and *Rhodobacterales* (Figure 1). To our knowledge, no functional data have been reported for this gene family other than results from a recent multi-species Tn-seq study that showed stress sensitivity in *Sinorhizobium meliloti* strains harboring transposon insertions in the DUF1849 gene, *SMc02102* (10). Here we show that in *Brucella*, the DUF1849 protein EipB (locus tag *bab1_1186*; RefSeq locus BAB_RS21600) is a 280-residue periplasmic protein that folds into a 14-stranded, open **β**-barrel containing a conserved disulfide bond. We term this novel barrel structure a **β**-spiral and show that it resembles the lipoprotein chaperone LolB, though its overall fold is distinct. Replication and survival of a *B. abortus* strain in which we deleted *eipB* was attenuated in a mouse infection model, and deletion of *eipB* in both *B. abortus* and *Brucella ovis* enhanced sensitivity to compounds that affect the integrity of the cell envelope. We have further shown that *B. abortus eipB* deletion is synthetically lethal with transposon disruption of *bab1_0430*, which encodes a periplasmic tetratricopeptide-repeat (TPR) protein that we have named TtpA. The *Brucella melitensis* ortholog of TtpA (locus tag BMEI1531) has been previously described as a molecular determinant of mouse spleen colonization (11), while a *Rhizobium leguminosarum* TtpA homolog (locus tag RL0936) is required for proper cell envelope function (12). We propose that TtpA and EipB coordinately function in the *Brucella* periplasm to ensure cell envelope integrity and to enable cell survival in the mammalian host niche.

Results

B. abortus eipB is required for maintenance of mouse spleen colonization

As part of a screen to evaluate the role of conserved *Alphaproteobacterial* genes of unknown function in *B. abortus* infection biology, we infected THP-1 macrophage-like cells with wild-type *B. abortus*, an *eipB* deletion strain (Δ*eipB*), and a genetically complemented Δ*eipB* strain. Infected macrophages were lysed and colony forming units (CFU) were enumerated on tryptic soy agar plates (TSA) at 1, 24 and 48 hours post-infection. We observed no significant differences

at 1, 24 or 48 hours post-infection, indicating that *eipB* was not required for entry, intracellular replication or survival *in vitro* (Figure 2A).

We further evaluated the role of *eipB* in a BALB/c mouse infection model. Mice infected with Δ*eipB* had no significant difference in spleen weight or bacterial load compared to mice infected with wild-type *B. abortus* strain 2308 at one-week post-infection (Figure 2B). However, at 4- and 8-weeks post-infection, mice infected with the wild-type or the complemented *eipB* deletion strains had pronounced splenomegaly and a bacterial load of approximately 5 x 10^6 CFU/spleen. In contrast, mice infected with Δ*eipB* had smaller spleens with approximately 2 orders fewer bacteria (~1 x 10^4 CFU/spleen) (Figure 2B). We conclude that *eipB* is not required for initial spleen colonization but is necessary for full virulence and persistence in the spleen over an 8-week time course.

To assess the pathology of mice infected with wild-type and Δ*eipB* strains, we harvested spleens at 8 weeks post-infection and fixed, mounted, and subjected the samples to hematoxylin and eosin (H&E) staining (Figure 3). Compared to naïve (uninfected) mice (Figure 3A), we observed higher extramedullary hematopoiesis, histiocytic proliferation, granulomas, and the presence of *Brucella* immunoreactivities in spleens of mice infected with wild-type *B. abortus* 2308 and the genetically-complemented mutant strain (Figure 3B and D). Both wild-type and the complemented strain caused spleen inflammation, with a reduced white to red pulp ratio as a result of lymphoid follicle disruption and red pulp expansion; these spleens also had increased marginal zones (Figure 3B and D). Mice infected with Δ*eipB* had reduced pathologic features: there was minimal change in white to red pulp ratio, and a minimal increase in marginal zones (Figure 3C). There was no evidence of extramedullary hematopoiesis in mice infected with Δ*eipB*, though histiocytic proliferation was mildly increased. Granulomas and *Brucella* immunoreactivities were rare in Δ*eipB* (Figure 3C). These results are consistent with a model in which *eipB* is required for full *B. abortus* virulence in a mouse model of infection. A summary of spleen pathology scores is presented in Table S1.

We further measured antibody responses in mice infected with Δ*eipB* and wild-type strains. Serum levels of total IgG, *Brucella*-specific IgG, IgG1, and IgG2a were measured by enzyme-linked immunosorbent assays (ELISA) (Figure 2C-F). At 8 weeks post-infection, total serum IgG was higher in all infected mice relative to the uninfected control (Figure 2C). The level of *Brucella*-specific IgG was approximately 6 times higher in Δ*eipB*-infected mice than in mice infected with wild-type or the complemented mutant strain (Figure 2D). Mice infected with wild-type, Δ*eipB* and the Δ*eipB*-complemented strain displayed similar increases in IgG1 and IgG2a at 8 weeks post infection (Figure 2E and F). We conclude that Δ*eipB* infection results in production of more *B. abortus*-specific antibodies. We did not test whether these antibodies contribute to clearance of the Δ*eipB* strain. Antibody production may simply be a consequence of antigen release triggered by host clearance of Δ*eipB* by other immune mechanisms.

The Δ*eipB* strain is sensitive to cell envelope stressors

To test whether reduced virulence of Δ*eipB* correlates with an increased sensitivity to stress *in vitro*, we evaluated *B. abortus* Δ*eipB* growth on TSA plates supplemented with known cell

membrane/envelope stressors including EDTA, ampicillin and deoxycholate. Δ*eipB* had 1.5 to 3 logs fewer CFU compared to wild-type when titered on TSA plates containing these compounds. All phenotypes were complemented by restoring the Δ*eipB* locus to wild-type (Figure 4A). Together, these data provide evidence that *eipB* contributes to resistance to compounds that compromise the integrity of the *B. abortus* cell membrane/envelope.

Although Δ*eipB* CFUs were reduced relative to wild-type on agar plates containing all three envelope stressors that we assayed, we observed no apparent defects in Δ*eipB* cell morphology by light microscopy or cryo-electron microscopy when cultivated in liquid broth (Figure 4B and C). Incubation of Δ*eipB* with 2 mM EDTA or 5 µg/ml ampicillin (final concentration) in Brucella broth for 4 hours also had no apparent effect on cell structure, nor did *eipA* overexpression (Figure 4B and C). Longer periods of growth in the presence of stressors may be required for differences in cell morphology/structure to be evident in broth. It may also be the case that the envelope stress phenotypes we observe are particular to growth on solid medium.

B. abortus Δ*eipB* agglutination phenotypes indicate the presence of smooth LPS
In *B. abortus*, smooth LPS (containing O-polysaccharide) is an important virulence determinant (13). Smooth LPS can also act as a protective layer against treatments that compromise the integrity of the cell envelope (14). Loss of smooth LPS in *B. abortus* Δ*eipB* could therefore explain the phenotypes we observe for this strain. To test this hypothesis, we assayed wild-type and Δ*eipB* agglutination in the presence of serum from a *B. abortus*-infected mouse. A major serological response to smooth *Brucella* species is to O-polysaccharide (15), and thus agglutination can provide an indirect indication of the presence or absence of smooth LPS on the surface of the cell. Both wild-type and Δ*eipB* strains agglutinated in the presence of serum, providing evidence for the presence of O-polysaccharide in Δ*eipB* (Figure 5A). As a negative control, we incubated the naturally rough species *B. ovis* with mouse serum; *B. ovis* did not agglutinate in the presence of serum (Figure 5A). We further assayed agglutination of *B. abortus* wild-type and Δ*eipB* strains in the presence of acriflavine, which is demonstrated to agglutinate rough strains such as *B. ovis* (16, 17). After 2 hours of incubation, we observed no agglutination of wild-type *B. abortus* or Δ*eipB* (Figure 5B). We treated *B. ovis* with acriflavine as a positive control and observed agglutination as expected (Figure 5B). Together, these data indicate that deletion of *eipB* does not result in a loss of smooth LPS. However, we cannot rule out the possibility that the chemical structure of O-polysaccharide is altered in Δ*eipB*.

EipB is a monomeric protein that is secreted to the periplasm
The N-terminus (residues M1-A30) of *Brucella* EipB contains a predicted signal peptide based on SignalP 4.2 analysis (18). EipB (DUF1849) homologs in other *Alphaproteobacteria* also have a predicted N-terminal secretion signal (Figure S1). We note that EipB in our wild-type *B. abortus* 2308 strain has a methionine instead of a leucine at position 250. These two amino acids are interchangeable at this position in DUF1849 (Figure S2). To test the prediction that EipB is a periplasmic protein, we fused the *Escherichia coli* periplasmic alkaline phosphatase gene (*phoA*) to *B. abortus eipB* and expressed fusions from a *lac* promoter in *B. ovis*. We generated (i) the full-length EipB protein (M1-K280) fused at its C-terminus to *E. coli* PhoA (EipB-PhoA$_{Ec}$) and (ii) an EipA-PhoA fusion lacking the hypothetical EipB signal peptide sequence (EipB$^{S29-K280}$-PhoA$_{Ec}$).

After overnight growth in Brucella broth in presence or absence of 1 mM isopropyl **β**-D-1-thiogalactopyranoside (IPTG), we adjusted each culture to the same density and loaded into a 96-well plate containing 5-bromo-4-chloro-3-indolyl phosphate (BCIP, final concentration 200 µg/ml). BCIP is hydrolyzed to a blue pigment by PhoA, which can be measured colorimetrically. BCIP diffusion through the inner membrane is inefficient, and thus this reagent can be used to specifically detect PhoA activity in the periplasmic space or in the extracellular medium (19). After a 2-hour incubation at 37°C, the well containing the *B. ovis* cells expressing the $EipB^{M1-K280}$-$PhoA_{Ec}$ fusion turned dark blue. We observed no color change in the well containing the *B. ovis* strain expressing the $EipB^{S29-K280}$-$PhoA_{Ec}$ protein fusion (Figure 6A). As expected, no color change was observed in absence of induction with 1 mM IPTG (Figure 6A). To test if EipB is secreted from the cell into the growth medium, we performed a similar experiment on spent medium supernatants from the different cultures. We observed no color change in these samples after 2 hours of incubation providing evidence that $EipB^{M1-K280}$-$PhoA_{Ec}$ is not secreted from the cell.

We further assayed the oligomeric state of affinity-purified *B. abortus* EipB in solution by size-exclusion chromatography. The calculated molecular mass of His_6-EipB (V31-K280) is 30.7 kDa. This protein eluted from a sizing column at a volume with an apparent molecular mass of ~23 kDa, which is consistent with a monomer (Figure 6B). There was no evidence of larger oligomers by size-exclusion chromatography. From these data, we conclude that EipB is likely a monomeric periplasmic protein.

EipB folds into a spiral-like **β**-sheet that resembles PA1994, LolA and LolB

We postulated that the three-dimensional structure of EipB may provide molecular-level insight into its function in the cell. As such, we solved an x-ray crystal structure of *B. abortus* EipB (residues A30-K280; PDB ID: 6NTR). EipB lacking its signal peptide formed triclinic crystals (a=47.4 Å b=69.2 Å, c=83.2 Å, ⍰=90.1, ⍰=90.0°, ⍰=78.7°) that diffracted to 2.1 Å resolution; we refined this structure to R_{work}= 0.195 and R_{free}= 0.245. Crystallographic data and refinement statistics are summarized in Table S2. Four EipB molecules (chains A-D) are present in the crystallographic asymmetric unit.

Each EipB monomer consists of 14 antiparallel **β**-strands, with **β**1-**β**12 and **β**14-**β**15 forming an oval, spiral-like **β**-sheet (minor axis diameter: ~25 Å; major axis diameter: ~35 Å). Two regions of this **β**-spiral, involving **β**5, **β**6, **β**7, **β**8 and the hairpin loop connecting **β**9 and **β**10, overlap (Figure 7A and B). Interactions between these two overlapping portions of structure are mostly hydrophobic, though polar contacts are also found in these regions (Figure 8A and B). One side of the spiral is occluded by **β**-strand 13 and **α**-helix 2, forming the bottom of this "cup" shaped protein. The external surface of EipB is positively and negatively charged, and also presents small hydrophobic patches (Figure S3); two helices, **α**1 (for which electron density is evident only in chains A and C) and **α**3, are positioned at the surface of the cylindrical **β**-spiral (Figure 7A and B). The lumen of EipB is solvent accessible and is partially filled with the side chains of hydrophobic or acidic residues. Hydrophobic residues represent ~52% of the residues present inside the EipB cavity (Figure 7 and 8). The size of this cavity suggests that EipB, in this conformation, can accommodate small molecules or ligands in its lumen.

We searched the Dali database (20) with the EipB structure, but failed to identify clear structural homologs. *Pseudomonas aeruginosa* PA1994 (PDB ID: 2H1T) (21) was the closest structural match to EipB (RMSD ~3.5; Z-score ~11) (Figure S4A). Despite very low sequence identity (~8%), PA1994 has noticeable structural similarities to EipB: it adopts a spiral-like **β**-fold involving 15 **β**-strands, which is occluded at one end with a long **α**-helix. Unlike EipB, PA1994 lacks a signal peptide and is predicted to be a cytoplasmic protein. Structural parallels between PA1994 and the periplasmic lipoprotein chaperones LolA/LolB have been noted and a role for PA1994 in glycolipid metabolism has been postulated (21), though this prediction remains untested. Like PA1994, EipB has structural similarities to LolA and LolB, in particular the antiparallel and curved β-sheet scaffold that engulfs a central **α**-helical plug (Figure S4B). Whether *Brucella* EipB, or DUF1849 proteins more generally, function in trafficking lipoproteins or other molecules in the periplasm also remains to be tested.

EipB has a conserved disulfide bond

We identified two cysteines in EipB, C69 and C278, which are the two most conserved residues in the DUF1849 sequence family (Figures S1 and S2). C69 is solvent exposed in *Brucella* EipB and positioned in a loop connecting **β**2 and **β**3. C278 is present at the C-terminus of the protein, which immediately follows **β**15. **β**15 interacts with **β**14 and **β**1, and is spatially proximal to **β**2 and **β**3 (Figure 9A). Given the proximity of these two cysteines in the EipB structure, we hypothesized that C69 and C278 could form an internal disulfide bond. However, electron density for the 10 C-terminal residues (containing C278) is not well resolved in the crystal structure, and a disulfide bond is not evident, likely because the protein was dialyzed against a buffer containing 2 mM 1,4-dithiothreitol (DTT) prior to crystallization.

To biochemically test if these two cysteines form a disulfide bond, we purified *B. abortus* EipB under non-reducing conditions and mixed the protein with SDS gel loading dye with and without 1 mM DTT. We observed two bands that migrated differently in the 30 kDa region when the protein was resolved by 12% SDS-PAGE. EipB incubated with DTT migrated farther than the untreated protein, suggesting the presence of a disulfide bond (Figure 9B). We performed this same experiment with three different EipB cysteine mutant proteins in which C69, C278, or both were mutated to serine. In the absence of DTT, $EipB^{C69S}$ and $EipB^{C278S}$ migrated at an apparent molecular weight of ~60 kDa, corresponding to a dimeric EipB interacting through an S-S bond. After DTT treatment, these mutant proteins migrated the same as the reduced wild-type protein (Figure 9B). As expected, the double cysteine mutant ($EipB^{C69S+C278S}$) did not form an apparent dimer and was unaffected by DTT (Figure 9B). From these data, we conclude that an internal disulfide bond can form between C69 and C278 in EipB and is likely present *in vivo*, as EipB resides in the oxidizing environment of the periplasm.

To test whether this disulfide bond affects EipB function, we measured CFU of a *Brucella ovis* Δ*eipB* strain expressing wild-type *B. abortus* EipB or cysteine disulfide mutants on agar plates containing 3 μg/ml carbenicillin. *B. ovis* is a closely related biosafety level 2 (BSL2) surrogate for *B. abortus*. *B. ovis* and *B. abortus* EipB are identical with the exception of one amino acid at position 250 (Figure S2). In this carbenicillin assay (Figure 9C and D), *B. abortus* EipB complemented a *B. ovis* Δ*eipB* strain, suggesting that the substitution at residue 250 does not

impair EipB function. We placed four different versions of *eipA* under the control of a *lac* promoter (P_{lac}): P_{lac}-*eipB*^{WT}, P_{lac}-*eipB*^{C69S}, P_{lac}-*eipB*^{C278S}, and P_{lac}-*eipB*$^{C69S+C278S}$; the empty vector was used as a control. After 5 to 6 days of growth on Schaedler Blood Agar (SBA) containing 3 µg/ml of carbenicillin and no IPTG, we observed poor growth at only the lowest dilution for wild-type and Δ*eipB* strains carrying the empty vector control. Corresponding colonies for strains carrying the different P_{lac}-*eipB* overexpression plasmids were more abundant though very small in the absence of IPTG induction. However, the strain harboring the wild-type *eipB* plasmid systematically grew at 1 log higher dilution than the cysteine mutant strains indicating that the presence of the disulfide bond in *eipB* contributes to carbenicillin resistance on solid medium (Figure 9C and D, see also Figure S5A). These results indicate some level of leaky expression from the multi-copy P_{lac}-*eipA* plasmids. When induced with IPTG, overexpression of the different EipB variants enhanced growth in all strains. (Figure 9C and D). As expected, strains grown on control plates without carbenicillin had no growth defect, with or without IPTG induction (Figure 9D). *B. ovis* Δ*eipB* strains expressing the different variants of *eipB* appeared normal by phase contrast microscopy (see Figure S5B). These results provide evidence that EipB is necessary for full carbenicillin resistance in *B. ovis*, and that cysteines 69 and 278 contribute to EipB function *in vivo*.

To evaluate the effect of these two cysteines on EipB stability *in vitro*, we measured the thermal stability of purified wild-type *B. abortus* EipB (EipB^{WT}) and double cysteine mutant (EipB$^{C692+C278S}$) in presence or absence of 2 mM DTT. EipB^{WT} melted at ~46°C in absence of DTT and at ~41.5°C in presence of DTT. EipB$^{C692+C278S}$ melted at ~42.3°C in the presence or absence of DTT (see Figure S6). We conclude that an internal disulfide bond stabilizes EipB structure *in vitro*. Reduced stability of EipB lacking its conserved disulfide bond may explain the 1 log relative growth defect of Δ*eipB* strains expressing EipB cysteine mutants on SBA carbenicillin (Figure 9C and D).

eipB deletion is synthetically lethal with *bab1_0430* (*ttpA*) disruption, and synthetically sick with disruption of multiple genes with cell envelope functions

To further characterize how *eipB* functions in the *Brucella* cell, we aimed to identify transposon (Tn) insertion mutations that are synthetically lethal with *eipB* deletion in *B. abortus* (see Tables S3 and S4). In other words, we sought to discover genes that are dispensable in a wild-type genetic background, but that cannot be disrupted in a Δ*eipB* background. By sequencing a Tn-Himar insertion library generated in *B. abortus* Δ*eipB* (NCBI Sequence Read Archive accession SRR8322167) and a Tn-Himar library generated in wild-type *B. abortus* (NCBI Sequence Read Archive accession SRR7943723), we uncovered evidence that disruption of *bab1_0430* (RefSeq locus BAB_RS17965) is synthetically lethal with *eipB* deletion. Specifically, reproducible reads corresponding to insertions in the central 10-90% of *bab1_0430* were not evident in Δ*eipB*, but were present in wild type (Figure 10A). *bab1_0430* encodes a 621-residue tetratricopeptide repeat-containing (TPR) protein that contains a predicted signal peptide and signal peptidase site at its N-terminus. This protein was previously detected by mass spectrometry analyses of *B. abortus* extracts, and described as a cell-envelope associated (22), or periplasmic protein (23). Hereafter, we refer to this gene as *ttpA* based on its similarity to *R. leguminosarum ttpA* (12).

Genes involved in LPS O-antigen synthesis, and previously described as synthetic lethal with *eipA* (*bab1_1612*) deletion in *B. abortus* (8), were synthetic sick with *eipB* deletion (Figure 10A), as were genes involved in peptidoglycan synthesis: *mltA* (*bab1_2076*, lytic murein transglycosylase A) and *bab1_0607* (glycosyl transferase/penicillin-binding protein) (24) (Figure 10A). There were reduced transposon insertions in solute binding protein *yejA1* (*bab1_0010*) (Figure 10A), which is involved in *B. melitensis* resistance to polymyxin (25). *lnt* (*bab1_2158*) and *vltR* (*bab1_1517*) were also synthetic sick with Δ*eipB*. *lnt* is an apolipoprotein N-acyltransferase involved in lipoprotein synthesis (26); *vltR* encodes a LysR transcriptional regulator required for full *B. abortus* virulence (27) (Figure 10A). Finally, the general stress sensor kinase *lovHK* (*bab1_0652*) (28), *bab1_1293* (homoserine dehydrogenase), and *bab1_0188* (methionine synthase), had fewer Tn insertions in the Δ*eipB* background relative to wild type (Figure 10A).

ttpA contributes to carbenicillin resistance

Transposon insertions in *ttpA* were the most detrimental insertions in a Δ*eipB* background, so we chose to further characterize this gene. All efforts to delete *B. ovis ttpA* (locus tag *bov_0411*) using a classic crossover recombination and *sacB* counterselection approach were unsuccessful, though hundreds of clones were screened. Efforts to delete the chromosomal copy by expressing a copy of *ttpA* from a plasmid also failed. This result is surprising considering that transposon insertions in *B. abortus ttpA* (NCBI Sequence Read Archive accession SRR7943723) and *B. ovis ttpA* (NCBI Sequence Read Archive accession SRR7943724) are tolerated (8). As an alternative approach to study the function of this gene, we inactivated *ttpA* using a single crossover recombination strategy. The corresponding *B. ovis* strain (Δ*ttpA*) was then transformed with a plasmid-borne IPTG-inducible copy of *ttpA* (pSRK-*ttpA*) or with an empty plasmid vector (EV). We evaluated sensitivity of these strains to carbenicillin by plating a dilution series on SBA plates containing 2.5 µg/ml carbenicillin, with or without IPTG inducer (Figure 10B and 10C). When compared to wild-type with empty vector, *B. ovis* Δ*ttpA* with empty vector had ~0.5 log reduced CFU on carbenicillin SBA. The corresponding colonies of *B. ovis* Δ*ttpA* were noticeably smaller than wild-type. Genetic complementation of Δ*ttpA* with pSRK-*ttpA* restored growth on carbenicillin plates. *B. ovis* Δ*ttpA*/pSRK-*ttpA* had ~1.5 log more colonies than wild-type in the presence of carbenicillin, with or without IPTG induction. Thus, leaky expression of *ttpA* from the *lac* promoter on pSRK-*ttpA* is apparently sufficient to protect this strain from carbenicillin on solid medium. Morphology of the *B. ovis* Δ*ttpA* strains appeared normal by phase contrast microscopy at 630x magnification (Figure S7).

To further evaluate the effect of *ttpA* overexpression, we assayed *B. ovis* wild-type and Δ*eipB* strains carrying pSRK-*ttpA*. As before, we tested sensitivity of these inducible expression strains to carbenicillin by plating a dilution series on SBA plates containing 3 µg/ml of carbenicillin, with or without 2 mM IPTG inducer (Figure 11A and B). Wild-type *B. ovis*/pSRK-*ttpA* and wild-type *B. ovis*/pSRK-*eipB* strains had equivalent CFU in the absence of carbenicillin, with or without IPTG. *ttpA* or *eipB* provided a ~3 log protective effect without IPTG induction in the presence of carbenicillin compared to the wild-type empty vector strain (Figure 11). Surprisingly, inducing *ttpA* expression with IPTG reduced its protective effect by 1 log on carbenicillin (relative to uninduced), and the corresponding colonies were very small suggesting slower growth under this condition (Figure 11B and C). This may be an effect of IPTG, based on reduced CFU counts of

wild-type empty vector control under this condition. As expected, induced expression of *eipB* from P_{lac}-*eipB* rescued the carbenicillin viability defect of Δ*eipB*. However, induced expression of *ttpA* from P_{lac}-*ttpA* was not sufficient to rescue the Δ*eipB* carbenicillin phenotype (Figure 11B and C). As before, we observed highly reduced CFU for *B. ovi*s wild-type or Δ*eipB* control strains carrying the pSRK empty vector (EV), when challenged with 3 µg/ml of carbenicillin. Morphology of wild-type or Δ*eipB B. ovis* strains overexpressing *ttpA* appeared normal by phase contrast microscopy at 630x magnification (Figure S8).

The observed genetic interaction between *eipB* and *ttpA* raised the possibility that their gene products physically interact. We tested interaction between EipB and TtpA proteins using bacterial two-hybrid and biochemical pull-down assays. We further evaluated whether a possible EipB-TtpA interaction is influenced by the presence or absence of the EipB internal disulfide bond using a biochemical pull-down. For our bacterial two-hybrid assay, $EipB^{V31-K280}$ was fused to the T25 adenylate cyclase fragment, and $TtpA^{K31-D621}$ was fused to the T18 or T18C adenylate cyclase fragments. For the pull-down assay, MBP-tagged TtpA (K31-D621) and His-tagged EipB (V31-K280; wild-type and the different cysteine mutants) were co-purified in presence or absence of DTT. We found no evidence for direct interaction between EipB and TtpA, suggesting that the function of these two proteins in *Brucella* envelope stress adaptation is not achieved through direct interaction (Figure S9).

DISCUSSION

Bacterial genome sequencing efforts over the past two decades have revealed thousands of protein domains of unknown function (DUFs). The DUF1849 sequence family is prevalent in orders *Rhizobiales*, *Rhodobacterales* and *Rhodospirillales* in the *Alphaproteobacteria*. To date, the function of this domain has remained undefined. In this study, we have shown that a DUF1849 gene in *Brucella* spp., named *eipB*, encodes a 14-stranded **β**-spiral protein that is secreted to the periplasm and that contains a conserved disulfide bond (Figures 9, S1 and S2). *eipB* is required for maintenance of *B. abortus* spleen colonization in a mouse model of infection (Figure 2), and *eipA* deletion in *B. abortus* and in *B. ovis* results in sensitivity to treatments that compromise the integrity of the cell envelope *in vitro* (Figure 3). Envelope stress sensitivity of the *B. abortus* Δ*eipB* mutant likely contributes to its reduced virulence in a mouse.

A lipoprotein connection?

An x-ray crystal structure of EipB shows that this periplasmic protein adopts an unusual **β**-spiral fold that shares structural similarity (DALI Z-score= 11.0) with a functionally-uncharacterized *P. aeruginosa* protein, PA1994, despite low sequence homology (Figure S4). It was previously noted that PA1994 has structural features that resemble the lipoprotein carrier and chaperone proteins LolA and LolB (21), which have a central role in lipoprotein localization in select Gram-negative bacteria (29). Like LolA, LolB, and PA1994, *Brucella* EipB forms a curved hydrophobic **β**-sheet that is wrapped around an **α**-helix (Figure S4B). Homologs of LolA are present in *Brucella* and other *Alphaproteobacteria*, but homologs of LolB are missing (26). Given the EipB structure, its periplasmic localization, and the phenotypes of a Δ*eipB* deletion strain it is tempting to speculate that EipB (DUF1849) has a LolB-like function in the *Brucella* cell. However, it seems unlikely that LolB and EipB function in a structurally- or biochemically-equivalent manner. Certainly, we

observe surface-level similarity between LolA/LolB and EipB structures (Figure S4), particularly in the antiparallel β-sheet region, but these proteins have topological differences that distinguish their folds. Moreover, LolB is a membrane anchored lipoprotein that facilitates lipoprotein targeting at the inner leaflet of the outer membrane. In contrast, *Brucella* EipB does not have a predicted site for lipidation (i.e. a lipobox), and is therefore unlikely to function as a membrane-anchored protein.

The number of uniquely barcoded Tn-Himar insertions in the apolipoprotein N-acyltransferase *lnt* (*bab1_2158*; *lnt* conserved domain database score < e^{-173}) is lower than expected in a Δ*eipB* background relative to wild-type (Figure 10A). This provides indirect evidence for a link between *eipB* and lipoproteins. Lnt catalyzes the final acylation step in lipoprotein biogenesis (30), which is often considered to be an essential biochemical process. However, like *Francisella tularensis* and *Neisseria gonorrhoeae* (31), *B. abortus lnt* is dispensable (24) (Figure 10A and Table S4). The data presented here suggest that transposon insertions are less tolerated in *B. abortus lnt* when *eipB* is missing. Additional experimentation is required to test a possible functional relationship between *lnt* and *eipB*. However, it is notable that we did not observe a synthetic genetic interaction between *lnt* and the gene encoding the structurally-unrelated periplasmic envelope integrity protein, EipA, in a parallel Tn-seq experiment (8). Whether *eipB* actually influences lipoprotein biogenesis or localization remains to be tested.

TtpA: a periplasmic determinant of cell envelope function in Rhizobiaceae
Transposon disruption of *ttpA* (*bab1_0430*) is not tolerated when *eipB* is deleted. Though there is a genetic interaction between *eipB* and *ttpA*, we found no evidence for a direct physical interaction between these two periplasmic proteins (Figure S9). Like *eipB*, *ttpA* influences *in vitro* sensitivity to carbenicillin (Figure 10B and C). TtpA contains a TPR motif. In bacteria, TPR proteins function in many different pathways including cell envelope biogenesis, and are often molecular determinants of virulence (32, 33). Deletion of *ttpA* attenuates *B. melitentis* virulence in a mouse infection model (11) and increases *R. leguminosarum* membrane permeability and sensitivity to SDS and hydrophobic antibiotics (12), respectively. A genetic interaction between *ttpA* and the complex media growth deficiency (*cmdA-cmdD*) operon has been reported in *R. leguminosarum*. Mutations in this operon result in envelope dysfunction and defects in cell morphology (12, 34). While *B. abortus* contains a predicted *cmd* operon (*bab1_1530, bab1_1531, bab1_1532, and bab1_1533*) these genes remain uncharacterized. We found no evidence for a synthetic genetic interaction between *eipB* and *cmd* in *B. abortus*, nor has such an interaction between *eipB* orthologs and *cmd* been reported in other *Rhizobiaceae*.

Notably, leaky expression of either *eipB* or *ttpA* from a plasmid strongly protected *B. ovis* from a cell wall antibiotic (carbenicillin). In the wild-type *B. ovis* background, we observed a phenomenon in which induced *ttpA* overexpression resulted in less protection against carbenicillin than low-level (leaky) expression (Figure 11A and B). Induced expression of *eipB* from a plasmid did not have this parabolic effect on cell growth/survival in the face of carbenicillin treatment. Considering that EipB and TtpA confer resistance to ampicillin and carbenicillin, two **β**-lactam antibiotics that inhibit synthesis of the peptidoglycan, one might hypothesize that these proteins influence the structure or synthesis of the cell wall. This

hypothesis is reinforced by the fact that a lytic murein transglycosylase and a class A PBP/glycosyl transferase were found to be synthetic sick with *eipB* deletion (Figure 10A). In *E. coli*, the TPR containing protein LpoA is proposed to reach from the outer membrane through the periplasm to interact with the peptidoglycan synthase PBP1A (35). Models in which EipB affects lipoprotein biosynthesis and/or cell wall metabolism are important to test as we work toward understanding how *eipB* functions to ensure *Brucella* cell envelope integrity and survival in a mammalian host.

Materials and Methods

Agglutination assays, mouse and macrophage infection assays and the transposon sequencing experiments for this study were performed in parallel with our recent studies of *eipA* (8).

All experiments using live *B. abortus* 2308 were performed in Biosafety Level 3 facilities according to United States Centers for Disease Control (CDC) select agent regulations at the University of Chicago Howard Taylor Ricketts Laboratory. All the *B. abortus* and *B. ovis* strains were cultivated at 37°C with 5% CO_2; primer and strain information is available in Table S5.

Chromosomal deletions in *B. abortus* and in *B. ovis*

The *B. abortus and B. ovis* Δ*eipB* deletion strains were generated using a double recombination strategy as previously described (8). Briefly, fragments corresponding to the 500 base pair upstream region of *eipB* start codon and the 500 base pair downstream region of *eipB* stop codon were ligated into the suicide plasmid pNPTS138 which carries the *nptI* gene for initial kanamycin selection and the *sacB* gene for counter-selection on sucrose. Genetic complementation of the *B. abortus* deletion strain was carried out by transforming this strain with the pNPTS138 plasmid carrying the wild-type allele locus. The *B. ovis* Δ*eipB* strain was complemented with the pSRK-*eipB* plasmid (IPTG inducible).

To inactivate *ttpA* in *B. ovis* (*bov_0411*), a 527-nucleotide long internal fragment was cloned into pNPTS138-*cam* (a suicide plasmid that we engineered to carry a chloramphenicol resistance marker) and used to disrupt the target gene by single crossover insertion. The recombinant clones were selected on SBA plates supplemented with 3 µg/ml chloramphenicol. This Δ*ttpA* strain was then complemented with pSRK-*ttpA*.

Brucella EipB and TtpA overexpression strains

For ectopic expression of *B. ovis* TtpA and the different versions of *B. abortus* EipB (wild-type, cysteine mutants, and the EipB-$PhoA_{Ec}$ fusion with or without the signal peptide), the pSRKKm (Kan^R) IPTG inducible plasmid was used (36). An overlapping PCR strategy was used to introduce cysteine mutations and to stitch the different DNA fragments to the *E. coli* alkaline phosphatase *phoA* (lacking its signal peptide). A Gibson-assembly cloning strategy was then used to insert the different DNA fragments in the linearized pSRK plasmid. After sequencing, plasmids were introduced in *B. abortus* or *B. ovis* by overnight mating with *E. coli* WM3064 in presence of 300 µM of diaminopimelic acid (DAP) and plated on SBA plates supplemented with kanamycin.

Building and mapping the wild-type *B. abortus* and *B. abortus* Δ*eipB* Tn-Himar insertion libraries

To build and map the different Tn-Himar insertion libraries, we used a barcoded transposon mutagenesis strategy developed by Wetmore and colleagues (37). A full and detailed protocol can be found in our previous paper (8). Statistics for the two different transposon insertion libraries are reported in Table S3. For each Himar insertion library, Tn-seq read data have been deposited in the NCBI sequence read archive: *B. abortus* 2308 wild-type (BioProject PRJNA493942; SRR7943723), *B. abortus* Δ*eipB* (Δ*bab1_1186*) (BioProject PRJNA510139; SRR8322167).

Cell culture and macrophage infection assay

Infection of inactivated macrophages differentiated from human monocytic THP-1 cells were performed as previously described (8). Briefly, for infection assays, 5 x 10^6 *B. abortus* cells were used to infect 5 x 10^4 THP-1 cells (multiplicity of infection of 1:100). To determine the numbers of intracellular bacteria at 1, 24 and 48 hours post-infection, the infected cells were lysed, the lysate was then serially diluted (10-fold serial dilution) and plated on TSA plates to enumerate CFU.

Mouse infection assay

All mouse studies were approved by the University of Chicago Institutional Animal Care and Use Committee (IACUC) and were performed as previously published (8). Briefly, 100 µl of a 5 x 10^5 CFU/ml *B. abortus* suspension were intraperitoneally injected into 6-week-old female BALB/c mice (Harlan Laboratories, Inc.). At 1, 4, and 8 weeks post-infection, 5 mice per strain were sacrificed, and spleens were removed for weighing and CFU counting. At week 8, blood was also collected by cardiac-puncture and serum from each mouse was separated from blood using a serum separation tube (Sarstedt). Sera were subsequently used for Enzyme-Linked ImmunoSorbent Assays (ELISA).

Determination of antibody responses at 8 weeks post infection

Total mouse serum IgG, IgG1, and IgG2a titers were measured using mouse-specific ELISA kits by following manufacturer's instructions (eBioscience). *Brucella*-specific IgG titers were determined as previously published (8).

Spleen histology

At 8 weeks post infection, spleens (n= 1 per strain) were prepared for histology as previously described (8). Briefly, spleens were first fixed with formalin and submitted for tissue embedding, Hematoxylin and Eosin (H & E) staining, and immunohistochemistry to Nationwide Histology (Veradale, Washington). For immunohistochemistry, goat anti-*Brucella* IgG was used (Tetracore, Inc). Pictures of fixed mouse spleen slides were subsequently analyzed and scored.

Plate stress assays

Stress assays were performed as previously published (8). Briefly, the different *B. abortus* and *B. ovis* strains were resuspended in sterile PBS or Brucella broth to an OD_{600} of ~ 0.015 (~ 1 x 10^8 CFU ml^{-1}) and serially diluted (10-fold serial dilution). 5 µl of each dilution were then spotted on TSA or SBA plates containing the different membrane stressors (2 to 5 µg/ml of ampicillin or carbenicillin, 200 µg/ml of deoxycholate or 2 mM EDTA).

To grow *B. ovis* strains containing pSRK-derived plasmids, all liquid cultures and plates were supplemented with 50 µg/ml kanamycin. When necessary, 2 mM of IPTG was added to the plates to induce ectopic expression of EipB or TtpA from pSRK. It is also important to note that the *B. ovis* Δ*ttpA* strains carry the pNPTS138 suicide plasmid (used for gene disruption) and are chloramphenicol resistant. However, no chloramphenicol was added to the overnight cultures or the stress plates. For carbenicillin growth/survival assays, strains were grown for 3 days at 37°C/ 5% CO_2 on SBA plates without carbenicillin, and for 5 to 6 days when these plates contained 2, 2.5 or 3 µg/ml of carbenicillin.

Cryo-electron microscopy

Cryo-electron microscopy was performed as previously described (8). Briefly, *B. abortus* cultures in Brucella broth (OD_{600} of ~0.015) were prepared with 2 mM EDTA or ampicillin (5 µg/ml) (final concentrations). After 4 hours of incubation in the presence of EDTA or ampicillin, cells were harvested and fixed in PBS + 4% formaldehyde. After 1 hour, cells were pelleted and resuspended in 500 µl EM buffer (38). Per CDC guidelines, cell killing was confirmed before sample removal for imaging. Fixed *Brucella* cells were vitrified on glow-discharged 200 mesh copper EM-grids with extra thick R2/2 holey carbon film (Quantifoil). Per grid, 3 µl of the sample was applied and automatically blotted and plunged into liquid ethane with the Leica EM GP plunge-freezer. Images were collected on a Talos L120C TEM (Thermo Fischer) using the Gatan cryo-TEM (626) holder. The images were acquired at a defocus between 8-10 µm, with a pixel size of 0.458 nm.

Light microscopy images

Phase-contrast images of *B. abortus* and *B. ovis* cells from plates or liquid broth (plus or minus 1 mM IPTG) were collected using a Leica DM 5000B microscope with an HCX PL APO 63×/1.4 NA Ph3 objective. Images were acquired with a mounted Orca-ER digital camera (Hamamatsu) controlled by the Image-Pro software suite (Media Cybernetics). To prepare the different samples, cells were resuspended in PBS containing 4% formaldehyde.

Agglutination assay

Agglutination assays were performed as previously described (8). The different *Brucella* strains (*B. ovis* and *B. abortus*) were harvested and resuspended in sterile PBS at OD_{600} ~ 0.5. One milliliter of each cell suspension was loaded in a spectrophotometer cuvette and mixed with 20 µl of wild-type *B. abortus*-infected mouse serum or with acriflavine (final concentration 5 mM) and ODs were measured at 600 nm at time (0) and after 2 hours. As a control, 1 ml of each cell suspension was also kept in a spectrophotometer cuvette without serum or acriflavine.

EipB expression, purification and crystallization

The DNA fragment corresponding to the *B. abortus* EipB protein (residues 31 - 280) was cloned into the pMCSG68 plasmid using a protocol previously published (8). For protein expression, an *E. coli* BL21-Gold(DE3) strain was used. Seleno-methionine protein expression and purification was performed as described (8). The purified protein was then dialyzed against 20 mM HEPES, pH 8.0, 250 mM NaCl, and 2 mM DTT buffer and its concentration was determined. The purified Se-Met EipB protein was concentrated to 160 mg/ml for crystallization. Initial crystallization

screening was carried out using the sitting-drop, vapor-diffusion technique. After a week, EipB crystallized in the triclinic space group P1 from the condition #70 of the MCSG-2 crystallization kit that contains 25% PEG1500 and 20% glycerol. Prior to flash freezing in liquid nitrogen, crystals were cryo-protected by briefly washing them in the crystallization solution containing 25% glycerol.

Crystallographic data collection and data processing

Se-Met crystal diffraction was measured at a temperature of 100 K using a 2-second exposure/degree of rotation and was collected for 260°. Crystals diffracted to a resolution of 2.1 Å and the corresponding diffraction images were collected on the ADSC Q315r detector with an X-ray wavelength near the selenium edge of 12.66 keV (0.97929 Å) for SAD phasing at the 19-ID beamline (SBC-CAT, Advanced Photon Source, Argonne, Illinois). Diffraction data were processed using the HKL3000 suite (39). *B. abortus* EipB crystals were twinned and the data had to be reprocessed and scaled from the $P2_1$ space group to the lower symmetry space group P1 with the following cell dimensions: a= 47.36 Å, b= 69.24 Å, c= 83.24 Å, and **α**= 90.09˚, **β**= 90.02˚, **γ**= 78.66˚ (see Table S2). The structure was determined by SAD phasing using SHELX C/D/E, mlphare, and dm, and initial automatic protein model building with Buccaneer software, all implemented in the HKL3000 software package (39). The initial model was manually adjusted using COOT (40) and iteratively refined using COOT, PHENIX (41), and/or REFMAC (42); 5% of the total reflections was kept out of the refinement in both REFMAC and PHENIX throughout the refinement. The final structure converged to an R_{work} of 19.5% and R_{free} of 24.5% and includes four protein chains (A: 30-270, B: 31-271, C: 30-271, and D: 30-270), 9 ethylene glycol molecules, two glycerol molecules, and 129 ordered water molecules. The EipB protein contained three N-terminal residues (Ser-Asn-Ala) that remain from the cleaved tag. The stereochemistry of the structure was checked using PROCHECK (43), and the Ramachandran plot and was validated using the PDB validation server. Coordinates of EipB have been deposited in the PDB (PDB code 6NTR). Crystallographic data and refined model statistics are presented in Table S2. Diffraction images have been uploaded to the SBGrid data server (Data DOI: 10.15785/SBGRID/445).

Alkaline phosphatase cell localization assay

To determine the cellular localization of EipB, we used a *B. ovis* strain transformed with the pSRK plasmid carrying *B. abortus eipB* C-terminally fused to *E. coli phoA*. Two versions of this plasmid were made: one carrying the full-length *eipB*, which expressed the protein with its signal peptide, and one carrying a short version of *eipB*, which expressed the protein lacking the signal peptide. Alkaline phosphatase assays were performed as previously described (8). Briefly, aliquots of overnight culture of *B. ovis* (in presence or absence of 1 mM IPTG) were mixed with 5-Bromo-4-chloro-3-indolyl phosphate (BCIP, final concentration 200 μM). After 2 hours of incubation, the color change was visually assessed and pictures were taken. Same experiment was performed with spent medium supernatants.

Size exclusion chromatography

A DNA fragment corresponding to *B. abortus eipB* lacking the signal peptide (residues 30 - 280) was cloned into pET28a and transformed into the protein overexpression *E. coli* Rosetta(DE3) *plysS* strain. Protein expression and purification was conducted using a Ni^{2+} affinity purification

protocol as previously published (8). The purified protein was then dialyzed against a Tris-NaCl buffer (10 mM Tris pH 7.4, 150 mM NaCl). EipB oligomeric state was analyzed by size exclusion chromatography as previously described. Briefly, after concentration, a protein sample (500 µl at 5 mg/ml) was injected onto a GE Healthcare Superdex 200 10/300 GL column (flow rate: 0.5 ml/min). Elution profile was measured at 280 nm and 500 µl fractions of were collected during the run; the dialyzing buffer as that described above was used for all runs. Protein standards (blue dextran / aldolase / conalbumin / ovalbumin) were also injected into the column, and the corresponding calibration curve was use for molecular size estimation of the purified EipB.

Pull-down assay between EipB and TtpA

To evaluate the interaction between *B. abortus* EipB and TtpA, the different proteins (His_6-$EipB^{WT}$ or His_6-EipB cysteine mutants, and MBP-TtpA) were overexpressed and purified using nickel affinity and amylose affinity gravity columns, respectively. Two milliliters of amylose resin were saturated with 10 ml of a clarified cell lysate corresponding to a 500 ml culture pellet of IPTG induced *Rosetta* pMalc2g-*ttpA*. Beads were thoroughly washed with 50 ml of a Tris-NaCl buffer (10 mM Tris pH7.4, 150 mM NaCl) and 200 µl of these beads were mixed with 500 µl of nickel purified EipB at ~0.5 mg/ml (see reference (8) for a detailed nickel-affinity purification protocol). After 30 min incubation in presence or absence of 1 mM DTT, the flow-through was saved and the beads were thoroughly washed with a Tris-NaCl buffer supplemented or not with 1 mM DTT. The protein was eluted with 200 µl of same buffer containing 20 mM of maltose. The different protein samples (elutions and flow-throughs) were run on a 12% SDS-PAGE and Coomassie stained.

Bacterial two-hybrid protein interaction assay

To assay EipB interaction with TtpA, we also used a bacterial two-hybrid system as previously published (8). Briefly, *B. abortus eipB* DNA fragments was cloned into pKT25 vector and *B. abortus ttpA* was cloned into pUT18 or pUT18C vectors. The different pUT18, pUT18C and pKT25 combinations were then co-transformed into chemically competent *E. coli* reporter strain BTH101 and spotted on LB agar plates (ampicillin 100 µg/ml + kanamycin 50 µg/ml) supplemented with X-Gal (40 µg/ml).

Disulfide bond reduction assays

DNA fragments corresponding to *B. abortus eipB* cysteine mutants (C69S, C278S, and C69S+C278S) and lacking the signal peptide (residues M1-A30) were cloned into pET28a and transformed into the protein overexpression *E. coli* Rosetta(DE3) *plysS* strain. Protein expression and Ni^{2+} affinity purification were conducted using protocols previously published (8). Briefly, for each protein, a pellet corresponding to a 250 ml culture was resuspended in 1.5 ml of BugBuster Master Mix (MD Millipore) supplemented with 50 µl of DNAse I (5mg/ml). After 20 min on ice, cell debris was pelleted and the supernatant was mixed with 200 µl of Ni-NTA Superflow resin (Qiagen). Beads were washed with 8 ml of a 10 mM imidazole Tris-NaCl buffer (10 mM Tris pH7.4, 150 mM NaCl) and 5 ml of a 75 mM imidazole Tris-NaCl buffer. Proteins were eluted with 200 µl of a 500 mM imidazole Tris-NaCl buffer. 50 µl of each purified protein (at 0.5 mg/ml) were then mixed with 12.5 µl of a 4x protein loading dye containing or not 1 mM of DTT. Samples were boiled for 5 min and 10 µl were loaded on a 12% SDS-PAGE.

Thermal shift protein stability assay

The thermal shift assay to assess protein stability was performed on 20 µl samples containing 25 µM of purified *B. abortus* EipB^{WT} or EipB$^{C69S+C278S}$, 50x Sypro Orange (Invitrogen) and 2 mM DTT when needed. Each protein sample and solution was prepared with the same dialysis buffer (10 mM Tris (pH 7.4), 150 mM NaCl, 1 mM EDTA). Ninety-six-well plates (MicroAmp EnduratePlate Optical 96-well fast clear reaction plates; Applied Biosystems) were used and heated from 25 to 95°C with a ramp rate of 0.05°C/s and read by a thermocycler (QuantumStudio 5 real-time PCR system; Applied Biosystems - Thermo Fisher scientific) using excitation and emission wavelengths of 470 ± 15 nm and 558 ± 11 nm, respectively. Protein Thermal Shift software v1.3 (Applied Biosystems - Thermo Fisher scientific) was used for calculation of the first derivative of the curve to determine the melting temperature.

Bioinformatics

Figures of the structures, structural alignments, electrostatic potential representations and r.m.s.d. calculations were performed using PyMOL (PyMOL Molecular Graphics System, version 1.7.4; Schrödinger, LLC). Surface hydrophobicity was evaluated using the YRB python script (44). The XtalPred server (45) and Dali server (46) were used to identify proteins with the highest structural and sequence homology. The BLAST server (https://blast.ncbi.nlm.nih.gov/Blast.cgi) was used to identify homologs of *B. abortus* EipB in different taxa within the *Alphaproteobacteria*. The weblogo was generated by aligning 447 *Alphaproteobacteria* DUF1849 protein sequences retrieved from the EMBL-EBI website (https://www.ebi.ac.uk/interpro/entry/IPR015000/proteins-matched). Alignment was generated with Clustal Omega (https://www.ebi.ac.uk/Tools/msa/clustalo/). When necessary, the C-terminus sequences were realigned by hand. The Clustal alignment file was then converted to a fasta file using http://sequenceconversion.bugaco.com/converter/biology/sequences/clustal_to_fasta.php. This file was then submitted to skylign server (http://skylign.org/) to generate a weblogo. The alignment was processed with the following options: remove mostly-empty columns / alignment sequences are full length / score.

Acknowledgments

We thank the members of the Crosson laboratory for helpful discussions. The authors wish to thank members of the SBC at Argonne National Laboratory for their help with data collection at the 19-ID beamline. This work was supported by National Institutes of Health Grants U19AI107792 and R01AI107159 to S.C.

Author contributions

JH, JWW and SC contributed to the design and conceptualization of the study; JH, JWW, AF, DMC, JXC, EU, AB, LB, GB, YK and SC performed the experiments, acquired and analyzed the data; JH, JWW, AF and SC interpreted the data; JH and SC wrote the original draft of the manuscript.

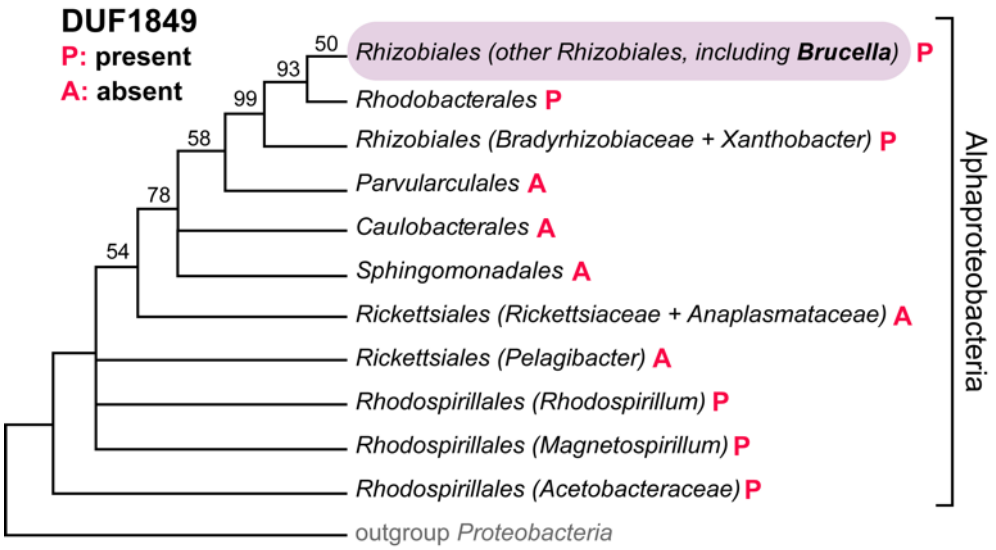

Figure 1: The DUF1849 sequence family is almost entirely restricted to *Alphaproteobacteria*. Bayesian phylogenetic tree showing the distribution of DUF1849 genes in different orders within the class *Alphaproteobacteria* (P: present, A: absent). Bayesian support values are shown when <100%; nodes were collapsed when support was <50%; adapted from Williams and colleagues (47). In *Brucella abortus* (order *Rhizobiales*), DUF1849 is encoded by gene locus *bab1_1186* (i.e. *eipB*).

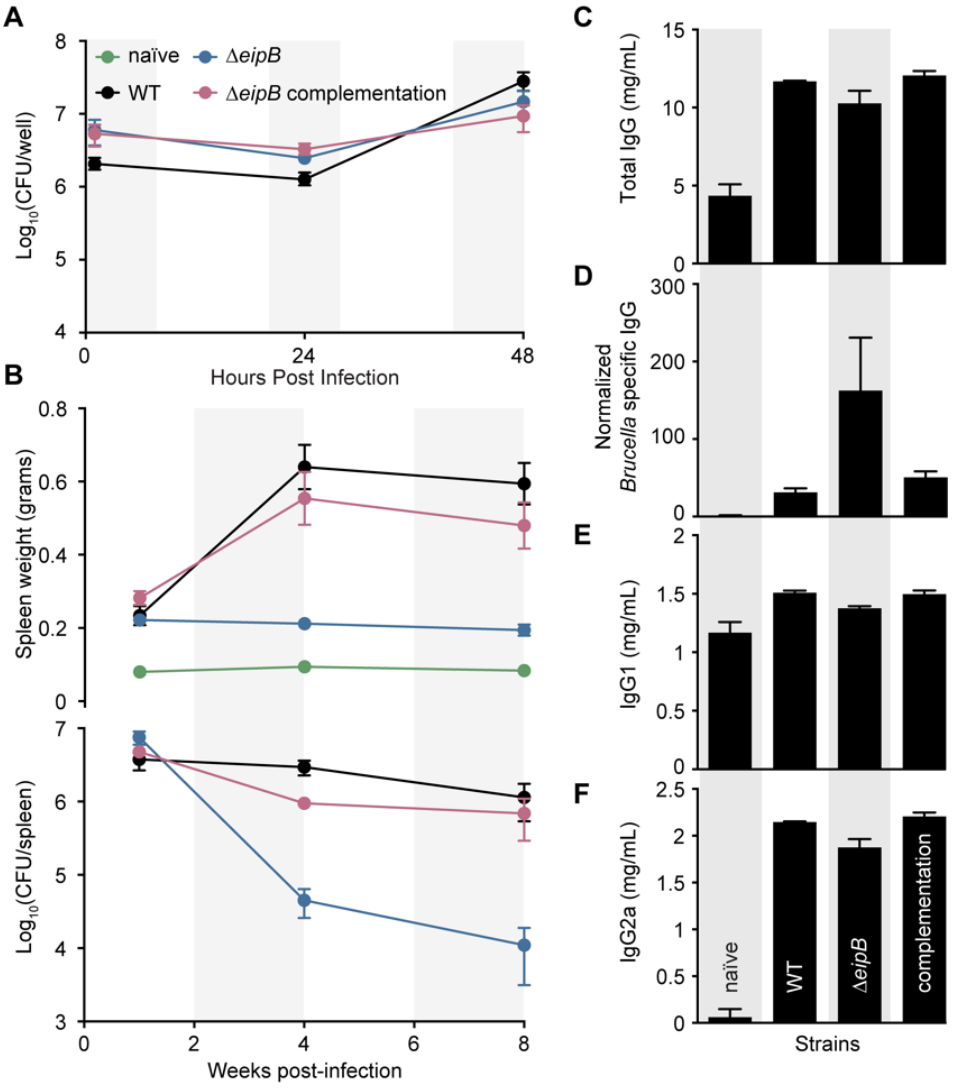

Figure 2: *eipB* is a genetic determinant of *B. abortus* virulence. A) *In vitro* macrophage infection assay: infection of THP-1 cells with wild-type *B. abortus* 2308 (black line), Δ*eipB* (blue line) and the *eipB* complementation strain (pink line). The number of *B. abortus* CFUs recovered from the THP-1 cells at 1, 24, and 48 hours post infection is plotted. Each data point (n= 3 per strain) is the mean ± the standard error of the mean. B) *In vivo* mouse infection assay: Female BALB/c mice were injected intraperitoneally with wild-type, Δ*eipB*, or Δ*eipB*-complementation strains. Spleen weights (upper graph) and bacterial burden (lower graph) were measured at 1, 4, and 8 weeks post-infection. Graphs represent data from uninfected, naïve mice (in green) or mice infected with wild-type (black), Δ*eipB* (blue), or complementation (pink) strains. Data presented are the mean ± the standard error of the mean; n= 5 mice per strain per time point. C-F) Antibody quantification in mouse serum harvested at 8 weeks post-infection from naïve control mice or mice infected with wild-type, Δ*eipB*, or complementation strains. Amounts of total IgG (C), *Brucella*-specific IgG (D), IgG1 (E), and IgG2a (F) were determined by ELISA. Each data point (naïve: n= 3, WT: n= 2, Δ*eipB* and complementation: n= 4) is the mean ± the standard error of the mean.

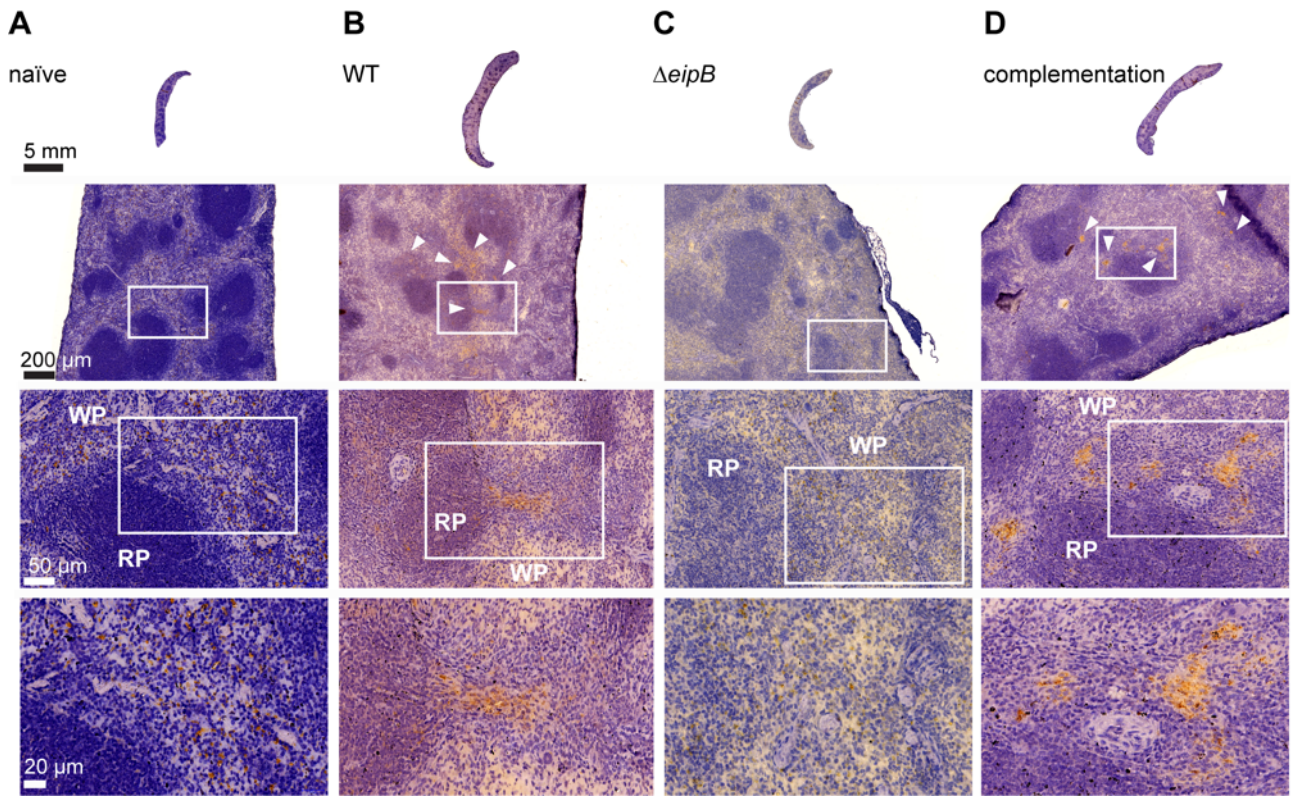

Figure 3: Histology of BALB/c mouse spleens at 8 weeks post-infection. Spleens (n= 1 per strain) were harvested, fixed, and stained with hematoxylin and eosin. Pictures of uninfected (A), wild-type (B), Δ*eipB* (C), or complementation (D) *B. abortus*-infected spleens were taken; white boxes represent specific regions enlarged in the images below. *Brucella* antigen was visualized by immunohistochemistry with an anti-*Brucella* antibody (brown regions, highlighted with white arrow heads). WP= white pulp, RP= red pulp.

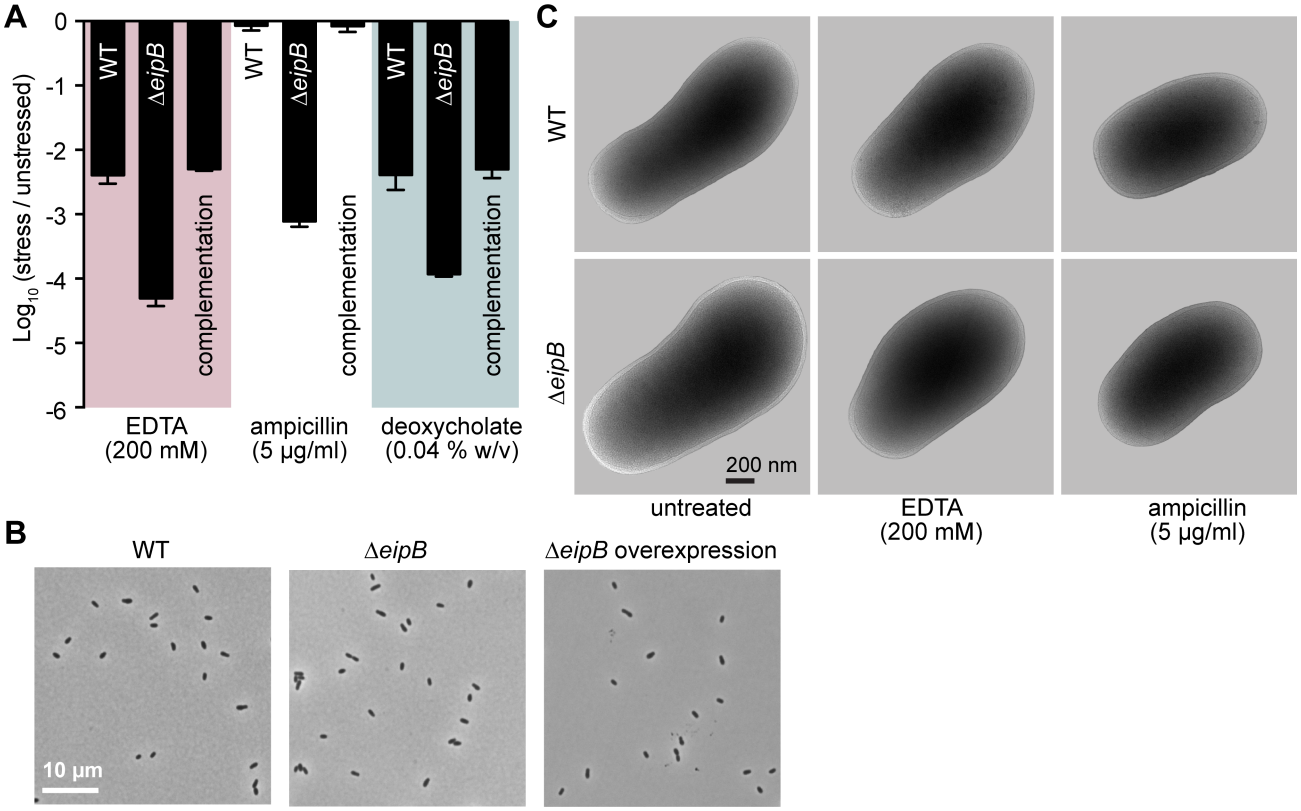

Figure 4: Assessing the effect of cell envelope stressors on *B. abortus* Δ*eipB* growth and survival. A) Envelope stress survival assays. Serially diluted cultures of *B. abortus* wild-type, Δ*eipB,* and complementation strains were spotted on plain TSA plates or TSA plates containing EDTA (2 mM), deoxycholate (0.04% w/v), or ampicillin (5 µg/ml). After 3 to 5 days of growth at 37°C / 5% CO_2, CFUs for each condition were enumerated and plotted. This experiment was repeated four times; each data point is the mean ± the standard error of the mean. B) Light micrograph of *B. abortus* wild-type (left), Δ*eipB* (middle) and overexpression (right; induced with 5 mM IPTG) liquid cultures grown overnight in Brucella broth. C) CryoEM images of *B. abortus* wild-type and Δ*eipB* cells cultivated in liquid broth that either remained untreated or were treated with 2 mM EDTA or 5 µg/ml ampicillin for 4 hours.

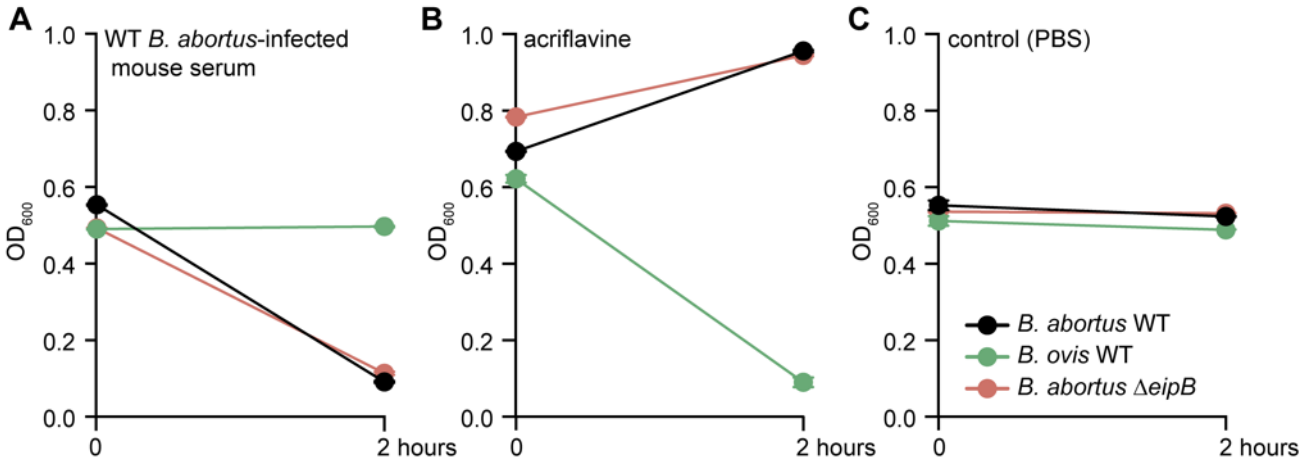

Figure 5: Deletion of *eipB* has no effect on the agglutination phenotype of *B. abortus*. The different *B. abortus* strains (wild-type in black, and Δ*eipB* in pink) and the wild-type *B. ovis* strain (in green) were incubated for 2 hours at room temperature in 1 ml of PBS supplemented with either (A) 20 µl of serum from a *B. abortus*-infected mouse, (B) 5 mM acriflavine (final concentration), or (C) no treatment. OD_{600} was measured at the beginning and the end of the experiment. The starting OD used was ~0.5. This experiment was performed in triplicate; each data point is the mean ± the standard error of the mean.

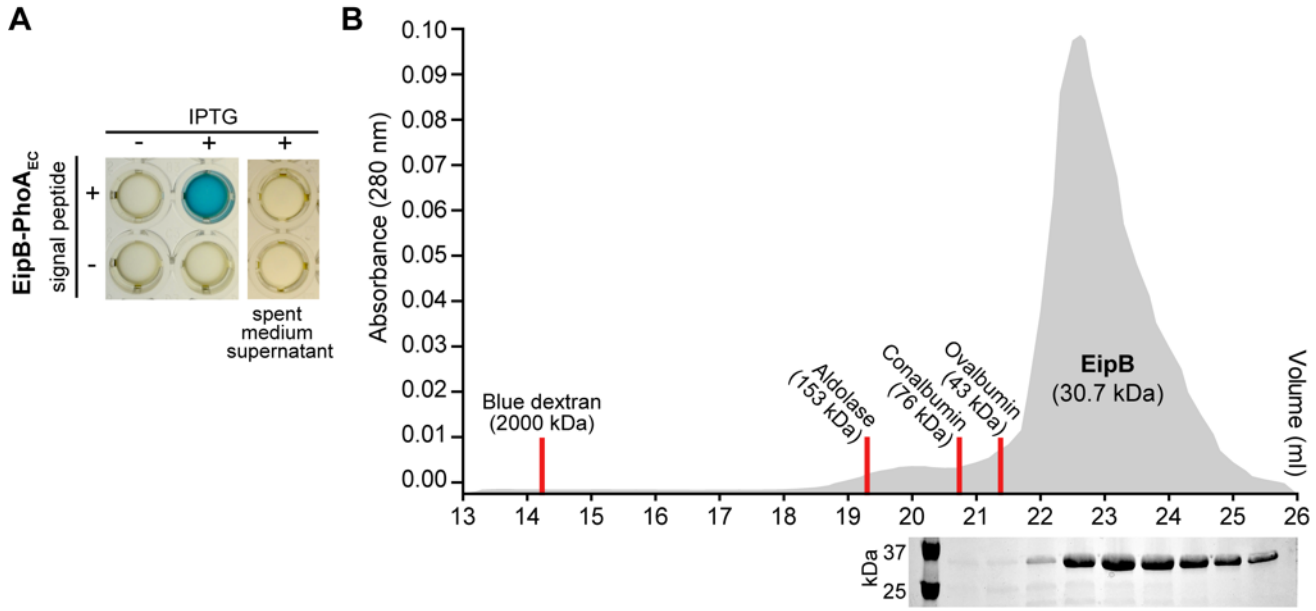

Figure 6: EipB is monomeric in solution and is secreted to the *Brucella* periplasm. A) Alkaline phosphatase assay. Overnight cultures of *B. ovis* expressing EipB with (+) or without (-) its signal peptide and fused to *E. coli* PhoA, were grown in presence (+) or absence (-) of 1 mM IPTG inducer. In a 96-well plate, these cultures were mixed with BCIP (200 µM final concentration) and developed for 2 hours at 37°C / 5% CO_2. Only the strain expressing EipB-PhoA$_{Ec}$ with a signal peptide turned blue, providing evidence that the protein is located in the periplasm. As a control, spent medium supernatants were mixed with BCIP to test whether EipB-PhoA$_{Ec}$ is secreted into the medium. After 2 hours incubation, no color change was observed, indicating that EipB-PhoA$_{Ec}$ is not exported outside the cell. These experiments were performed at least three times with independent clones. A representative image is shown. B) Size exclusion chromatography elution profile of purified EipB (in grey). Elution fractions were loaded on a SDS-PAGE, and a single band migrating at ~30 kDa was visible. Elution peaks of the molecular weight standards (blue dextran: 2000 kDa, aldolase: 157 kDa, conalbumin: 76 kDa, ovalbumin: 43 kDa) are shown as red line. This experiment was performed twice and yielded similar elution profiles.

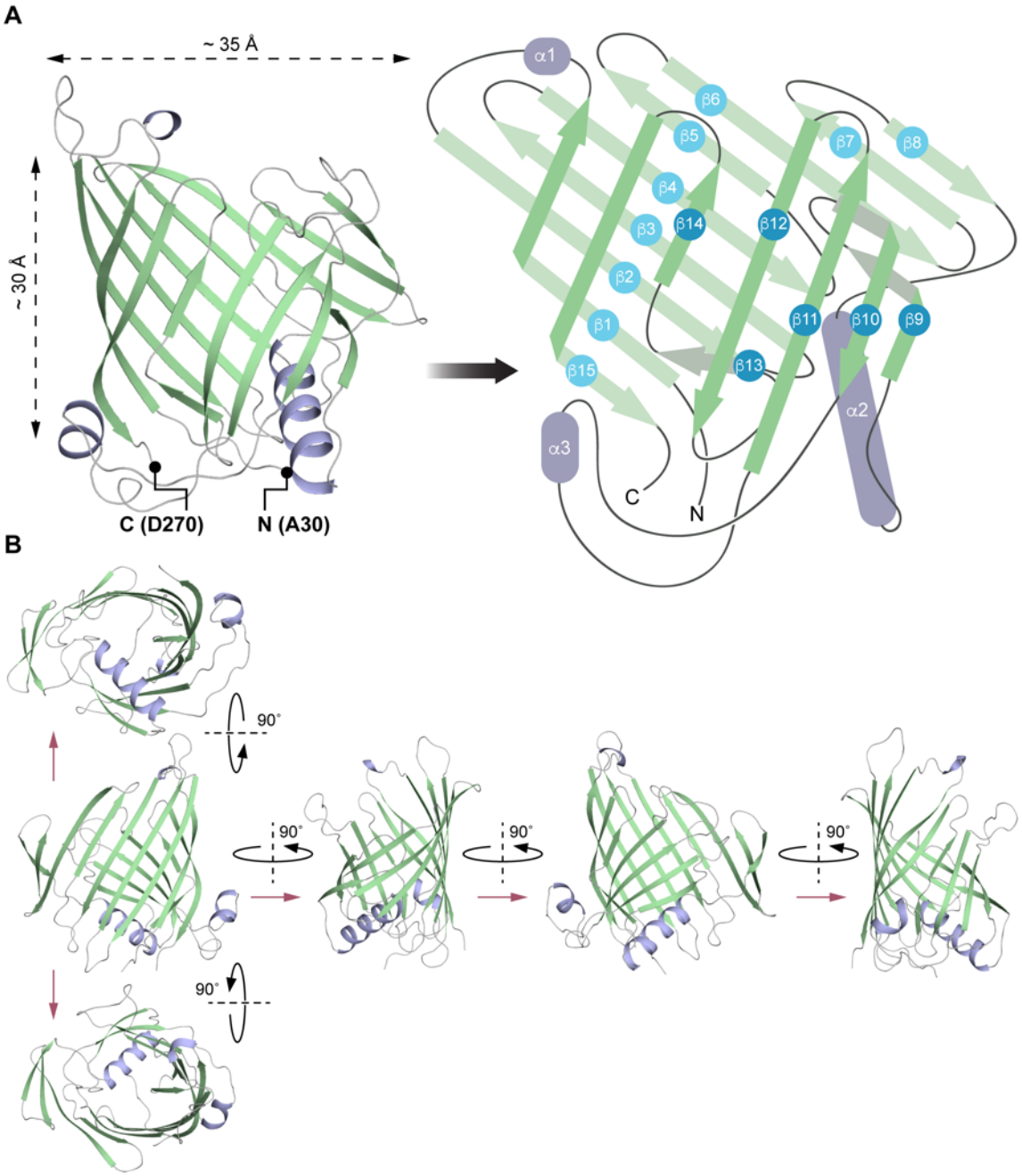

Figure 7: EipB adopts a **β**-spiral fold. A) Left: X-ray structure of EipB. EipB consist of 15 **β**-strands (in green) and 3 **α**-helices (in violet). The N-terminus (A30) and the C-terminus (D270) are reported on this structure. Right: simplified representation of EipB; color code is the same as before. B) Different orientations of EipB structure; color code is the same as before.

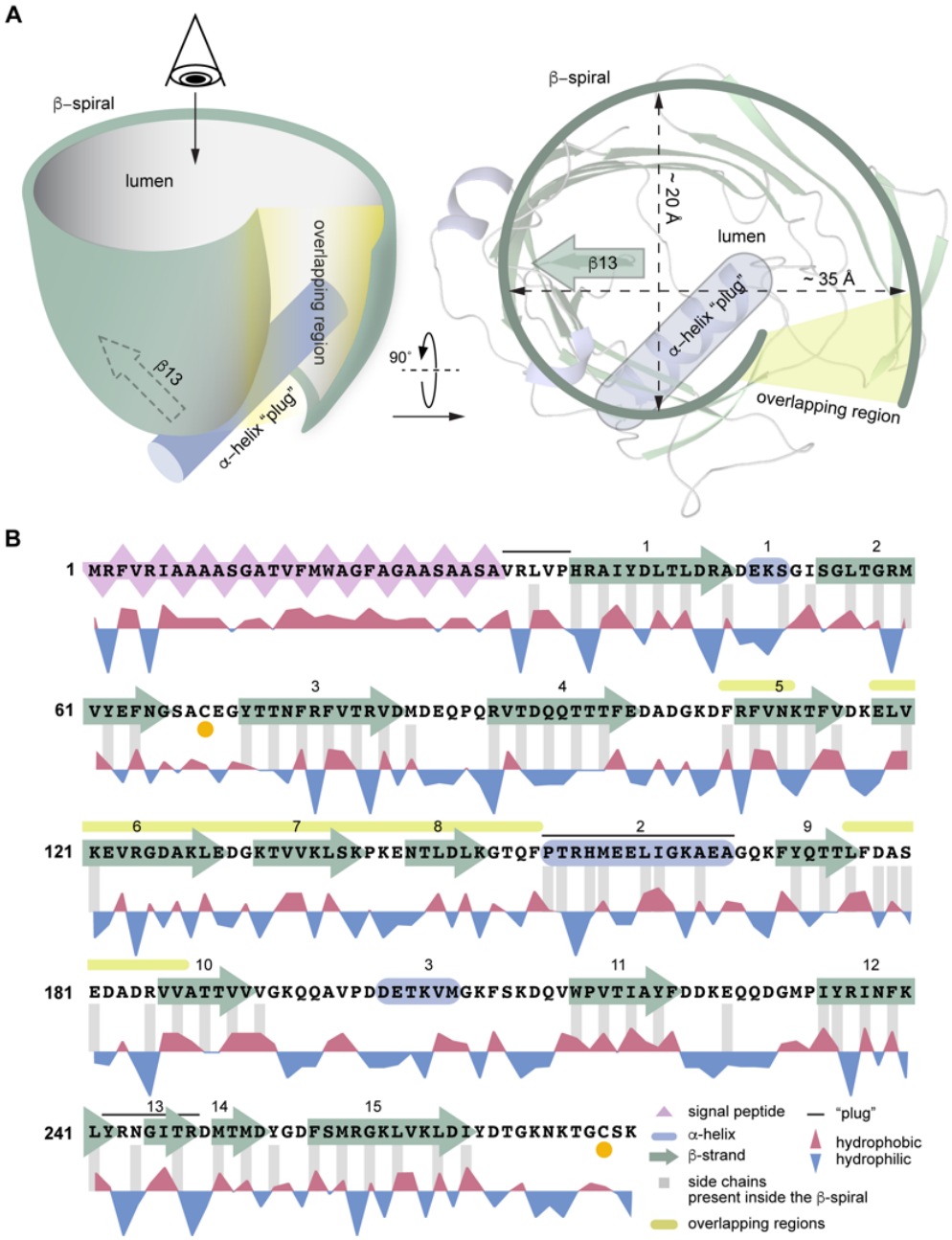

Figure 8: Simplified representation of EipB structure. A) EipB adopts a cup-like structure, fourteen **β**-strands (in green) form an overlapping **β**-spiral (**β**5-**β**6-**β**7-**β**8 overlap with **β**9-**β**10 connecting loop, highlighted in yellow in panel A and B). **α**2 (in violet) and **β**13 (in green) form the bottom of this "cup". B) Amino acid sequence of EipB. The sequence corresponding to the predicted signal peptide is highlighted in pink. **β**-strands and **α**-helices are represented by green arrows and violet cylinders, respectively. Hydrophobic (red) and hydrophilic (blue) residues are reported below the sequence. Residues with side chains present inside EipB cavity are highlighted with grey bars. Cysteines C69 and C278 are highlighted with orange dots.

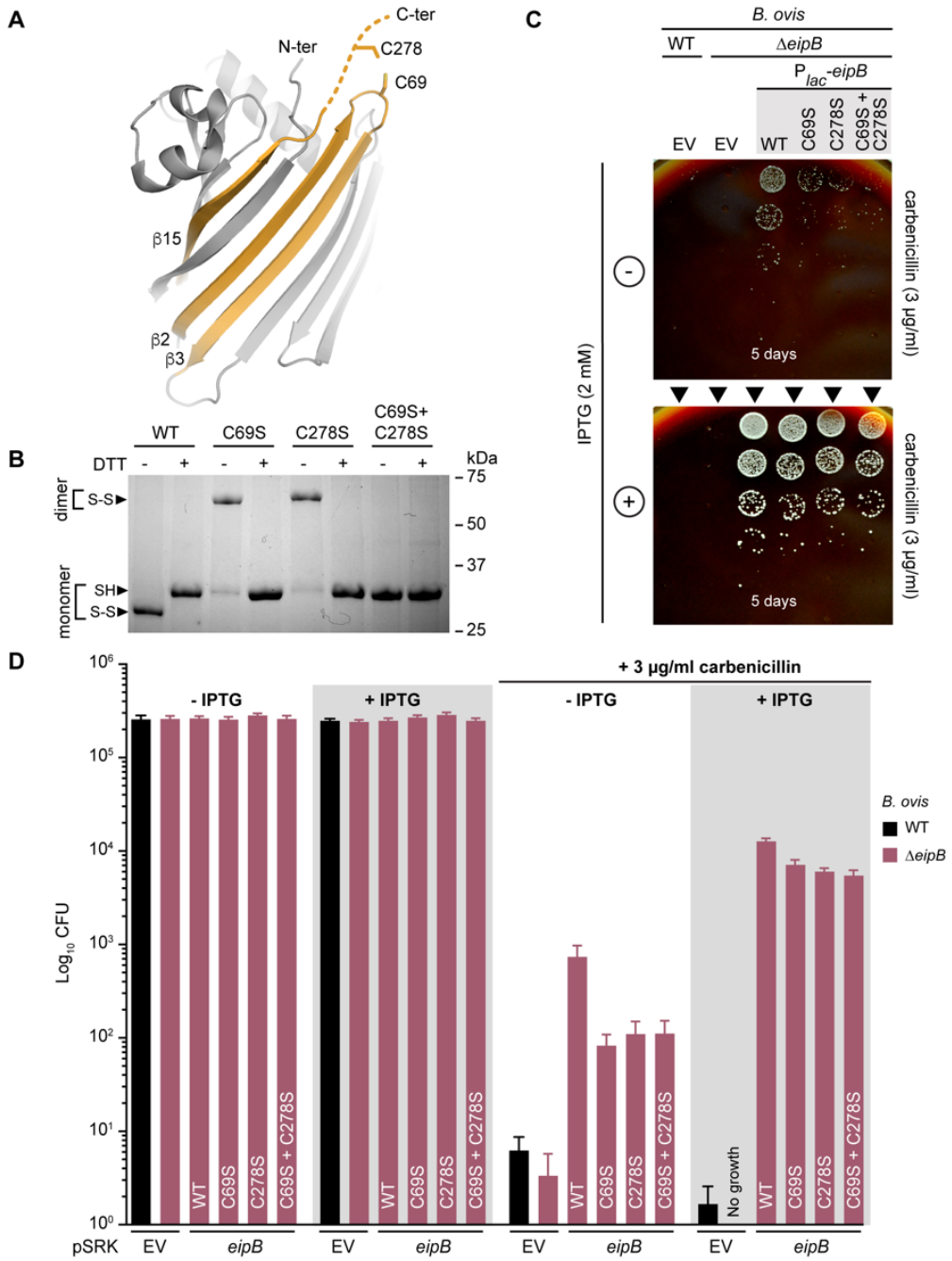

Figure 9: EipB has an internal disulfide bond. A) Cysteines C69 and C278 are spatially proximal in the EipB structure and form a disulfide bond. C278 is present at the EipB C-terminus that follows **β**15, and C69 is present in a loop connecting **β**2 and **β**3. B) His-tagged wild-type EipB and EipB cysteine mutant proteins (C69S, C278S, and C69S+C278S) were purified and mixed with a protein loading buffer plus or minus 1 mM DTT. Protein samples were resolved by 12% SDS-PAGE. This experiment was performed three times. Picture of a representative gel is presented. C) Growth on SBA plates containing 3 µg/ml of carbenicillin ± 2 mM IPTG of a serially diluted (10-fold dilution) *B. ovis* Δ*eipB* strain ectopically expressing wild-type EipB (P_{lac}-*eipB*), C69S mutant (P_{lac}-*eipB*^{C69S}), C278S mutant (P_{lac}-*eipB*^{C69S}), or C69S+C278S mutant (P_{lac}-*eipB*$^{C69S+C278S}$). *B. ovis* wild-type (WT) and Δ*eipB* carrying the pSRK empty vector (EV) was used as a control. Days of growth

at 37°C / 5% CO_2 are reported for each plate. A representative picture of the different plates is presented. D) Enumerated CFU after growth on SBA plates containing 3 µg/ml of carbenicillin ± 2 mM IPTG of serially diluted (10-fold dilution) *B. ovis* Δ*eipB* strains expressing different versions of *eipB* from a plasmid (wild-type and cysteine mutants; see panel C legend). Empty vector (EV) strains and SBA plates with no carbenicillin, plus or minus IPTG, were used as controls. This experiment was independently performed twice with two different clones each time, and all plate assays were done in triplicate. Each data point is the mean ± the standard error of the mean.

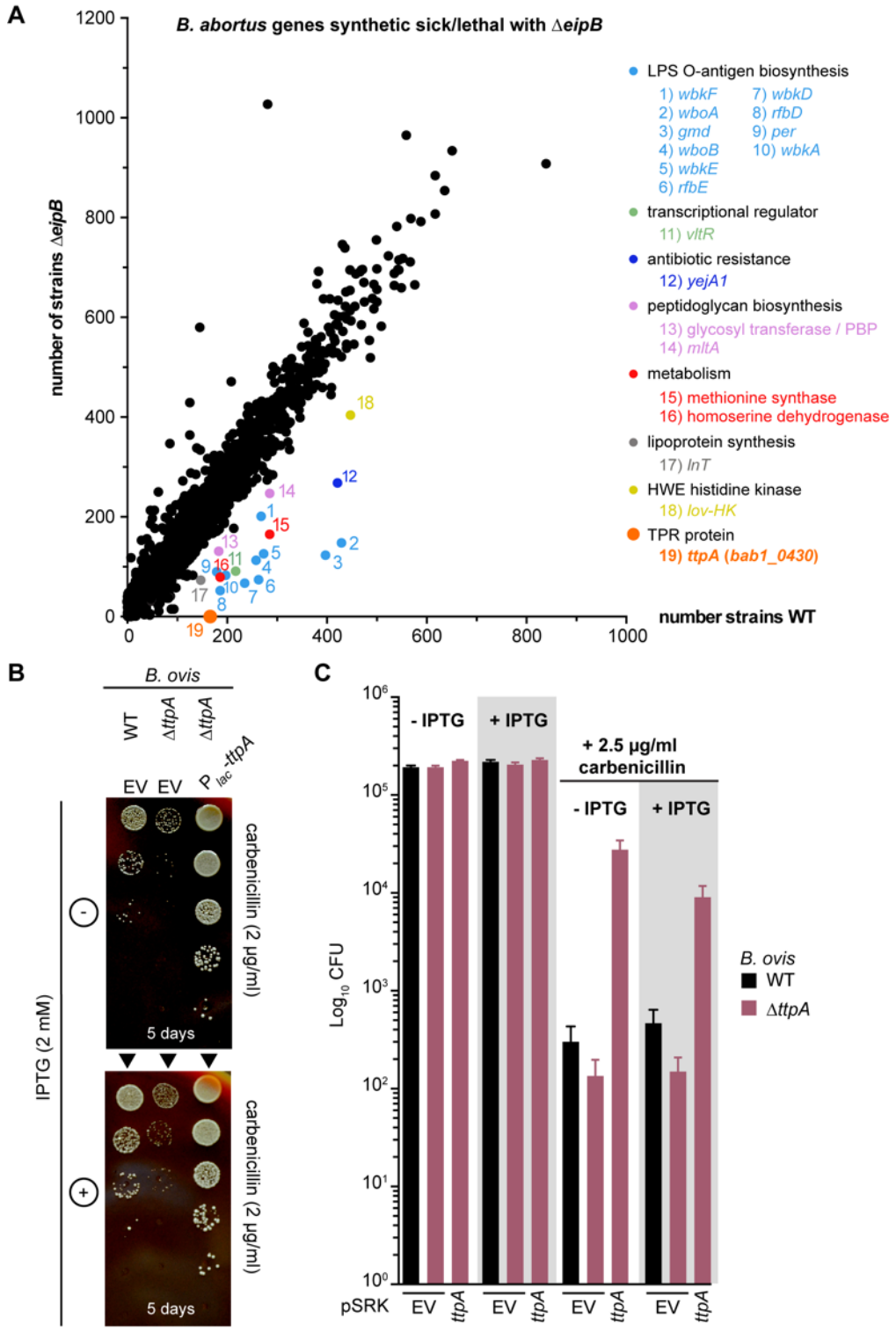

Figure 10: *B. abortus eipB* deletion is synthetically lethal with Tn-Himar disruption of *bab1_0430*, which encodes a TPR protein. A) Identification of *B. abortus* genes that are synthetically lethal or sick with *eipB* deletion. Tn-Himar insertion strains per gene (black dots) obtained in a *B. abortus*

Δ*eipB* background are plotted as a function of strains per gene in a wild-type background. *bab1_0430*, for which we observed significantly fewer insertions in Δ*eipB* than in wild-type, is represented as an orange dot. Other synthetic sick genes are also evident in the plot, including genes involved in LPS O-antigen synthesis in light-blue (*wbkF bab1_0535*; *wboA bab1_0999*; *gmd bab1_0545*; *wboB bab1_1000*; *wbkE bab1_0563*; *rfbE bab1_0542*; *wbkD, bab1_0534*; *rfbD bab1_0543*; *per bab1_0544*; *wbkA bab1_0553*), genes related to peptidoglycan synthesis in pink (*mltA bab1_2076*; penicillin-binding protein *bab1_607*). Apolipoprotein N-acyltransferase *lnt* (*bab1_2158*) is in grey; LysR transcriptional regulator *vtlR* (*bab1_1517*) is in light green; extracellular solute binding protein *yejA1* (*bab1_0010*) is in dark blue; general stress response regulator *lovhK* (*bab1_0652*) is in yellow; metabolic genes (methionine synthase *bab1_0188*, and homoserine dehydrogenase *bab1_1293*) are in red. B) Growth on SBA plates containing 2 µg/ml of carbenicillin ± 2 mM IPTG of serially diluted (10-fold dilution) *B. ovis* Δ*ttpA* strains carrying the pSRK empty vector (EV) or ectopically expressing wild-type TtpA (P_{lac}-*ttpA*). The wild-type (WT) *B. ovis* pSRK empty vector (EV) strain was used as a control. Days of growth at 37°C / 5% CO_2 are reported for each plate. A representative picture of the different plates is presented. C) Enumerated CFU, after growth on SBA plates containing 2.5 µg/ml of carbenicillin ± 2 mM IPTG, of serially diluted (10-fold dilution) *B. ovis* wild-type (black) and Δ*ttpA* (dark pink) strains. The Δ*ttpA* strain was either transformed with the empty vector (EV) or with pSRK-*ttpA*. Empty vector (EV) wild-type strain and SBA plates with no carbenicillin, and plus or minus IPTG were used as controls. This experiment was independently performed twice with two different clones each time, and all plate assays were done in triplicate. Each data point is the mean ± the standard error of the mean.

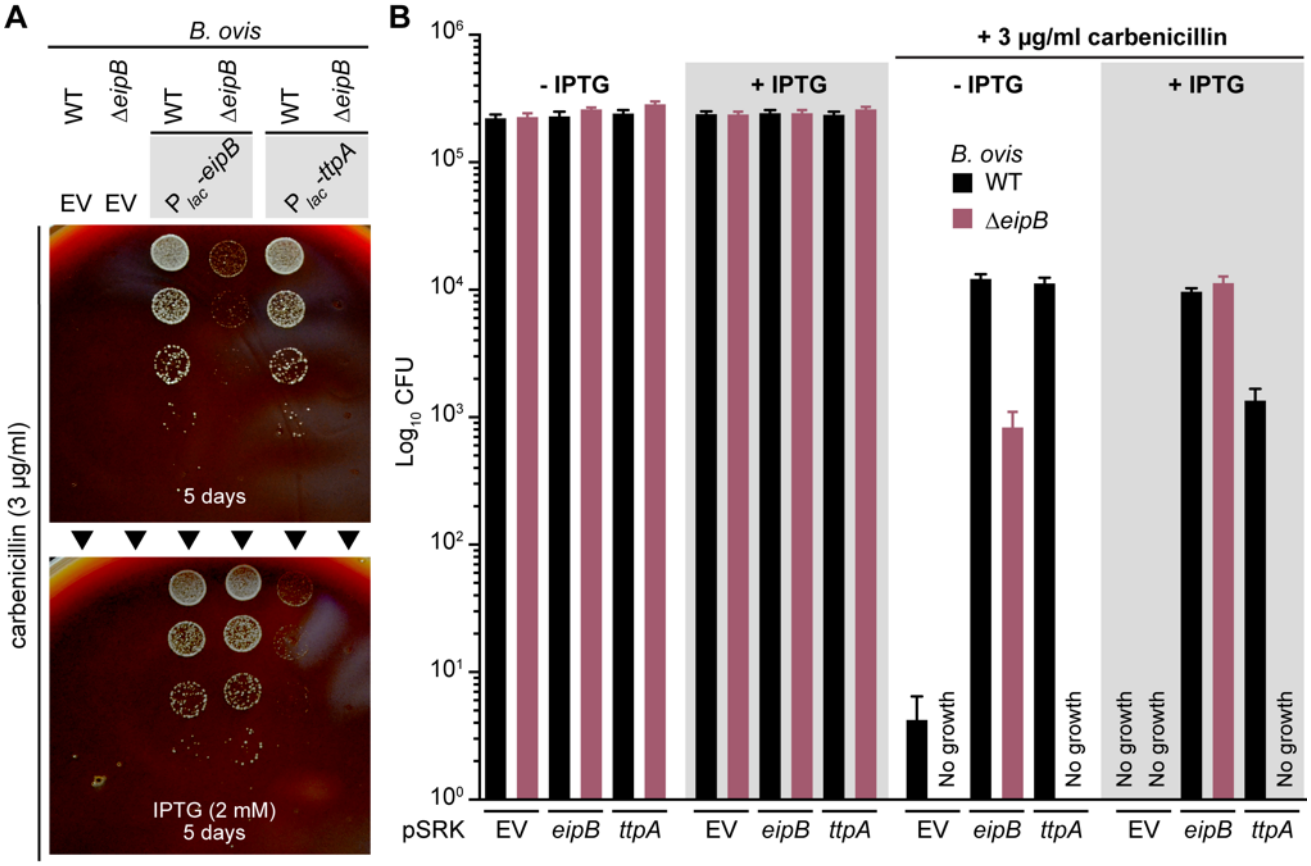

Figure 11: Overexpression of TtpA protects against carbenicillin treatment; protection requires EipB. A) Growth on SBA plates containing 3 µg/ml of carbenicillin ± 2 mM IPTG of serially diluted (10-fold dilution) *B. ovis* wild-type (WT) and Δ*eipB* strains expressing wild-type EipB (P_{lac}-*eipB*) or TtpA (P_{lac}-*ttpA*). *B. ovis* strains carrying the pSRK empty vector (EV) were used as a control. Days of growth at 37°C / 5% CO_2 are reported for each plate. A representative picture of the different plates is presented. B) Enumerated CFU after growth on SBA plates containing 3 µg/ml of carbenicillin ± 2 mM IPTG of serially diluted (10-fold dilution) *B. ovis* wild-type (black) and Δ*eipB* (dark pink) strains ectopically expressing *eipB* or *ttpA*. Empty vector (EV) strains and SBA plates with no carbenicillin, and plus or minus IPTG were used as controls. This experiment was independently performed twice with two different clones each time, and all plate assays were done in triplicate. Each data point is the mean ± the standard error of the mean.

References

1. Gorvel JP, Moreno E. 2002. *Brucella* intracellular life: from invasion to intracellular replication. Vet Microbiol 90:281-97.
2. Pappas G, Papadimitriou P, Akritidis N, Christou L, Tsianos EV. 2006. The new global map of human *brucellosis*. Lancet Infect Dis 6:91-9.
3. Batut J, Andersson SG, O'Callaghan D. 2004. The evolution of chronic infection strategies in the alpha-proteobacteria. Nat Rev Microbiol 2:933-45.
4. Atluri VL, Xavier MN, de Jong MF, den Hartigh AB, Tsolis RM. 2011. Interactions of the human pathogenic *Brucella* species with their hosts. Annu Rev Microbiol 65:523-41.
5. Roop RM, 2nd, Gaines JM, Anderson ES, Caswell CC, Martin DW. 2009. Survival of the fittest: how Brucella strains adapt to their intracellular niche in the host. Med Microbiol Immunol 198:221-38.
6. Byndloss MX, Tsolis RM. 2016. Brucella spp. Virulence Factors and Immunity. Annu Rev Anim Biosci 4:111-27.
7. Lamontagne J, Butler H, Chaves-Olarte E, Hunter J, Schirm M, Paquet C, Tian M, Kearney P, Hamaidi L, Chelsky D, Moriyon I, Moreno E, Paramithiotis E. 2007. Extensive cell envelope modulation is associated with virulence in Brucella abortus. J Proteome Res 6:1519-29.
8. Herrou J, Willett JW, Fiebig A, Varesio LM, Czyz DM, Cheng JX, Ultee E, Briegel A, Bigelow L, Babnigg G, Kim Y, Crosson S. 2018. Periplasmic protein EipA determines envelope stress resistance and virulence in *Brucella abortus*. Mol Microbiol doi:10.1111/mmi.14178.
9. Finn RD, Coggill P, Eberhardt RY, Eddy SR, Mistry J, Mitchell AL, Potter SC, Punta M, Qureshi M, Sangrador-Vegas A, Salazar GA, Tate J, Bateman A. 2016. The Pfam protein families database: towards a more sustainable future. Nucleic Acids Res 44:D279-85.
10. Price MN, Wetmore KM, Waters RJ, Callaghan M, Ray J, Liu H, Kuehl JV, Melnyk RA, Lamson JS, Suh Y, Carlson HK, Esquivel Z, Sadeeshkumar H, Chakraborty R, Zane GM, Rubin BE, Wall JD, Visel A, Bristow J, Blow MJ, Arkin AP, Deutschbauer AM. 2018. Mutant phenotypes for thousands of bacterial genes of unknown function. Nature 557:503-509.
11. Lestrate P, Dricot A, Delrue RM, Lambert C, Martinelli V, De Bolle X, Letesson JJ, Tibor A. 2003. Attenuated signature-tagged mutagenesis mutants of *Brucella melitensis* identified during the acute phase of infection in mice. Infect Immun 71:7053-60.
12. Neudorf KD, Vanderlinde EM, Tambalo DD, Yost CK. 2015. A previously uncharacterized tetratricopeptide-repeat-containing protein is involved in cell envelope function in *Rhizobium leguminosarum*. Microbiology 161:148-57.
13. Lapaque N, Moriyon I, Moreno E, Gorvel JP. 2005. *Brucella* lipopolysaccharide acts as a virulence factor. Curr Opin Microbiol 8:60-6.
14. Papo N, Shai Y. 2005. A molecular mechanism for lipopolysaccharide protection of Gram-negative bacteria from antimicrobial peptides. J Biol Chem 280:10378-87.
15. Palmer DA, Douglas JT. 1989. Analysis of *Brucella* lipopolysaccharide with specific and cross-reacting monoclonal antibodies. J Clin Microbiol 27:2331-7.
16. Alton GG, Jones LM, Pietz DE. 1975. Laboratory techniques in brucellosis. Monogr Ser World Health Organ:1-163.
17. Turse JE, Pei J, Ficht TA. 2011. Lipopolysaccharide-Deficient Brucella Variants Arise Spontaneously during Infection. Front Microbiol 2:54.

18. Nielsen H. 2017. Predicting Secretory Proteins with SignalP. Methods Mol Biol 1611:59-73.
19. Marrichi M, Camacho L, Russell DG, DeLisa MP. 2008. Genetic toggling of alkaline phosphatase folding reveals signal peptides for all major modes of transport across the inner membrane of bacteria. J Biol Chem 283:35223-35.
20. Holm L, Laakso LM. 2016. Dali server update. Nucleic Acids Res 44:W351-5.
21. Bakolitsa C, Kumar A, McMullan D, Krishna SS, Miller MD, Carlton D, Najmanovich R, Abdubek P, Astakhova T, Chiu HJ, Clayton T, Deller MC, Duan L, Elias Y, Feuerhelm J, Grant JC, Grzechnik SK, Han GW, Jaroszewski L, Jin KK, Klock HE, Knuth MW, Kozbial P, Marciano D, Morse AT, Nigoghossian E, Okach L, Oommachen S, Paulsen J, Reyes R, Rife CL, Trout CV, van den Bedem H, Weekes D, White A, Xu Q, Hodgson KO, Wooley J, Elsliger MA, Deacon AM, Godzik A, Lesley SA, Wilson IA. 2010. The structure of the first representative of Pfam family PF06475 reveals a new fold with possible involvement in glycolipid metabolism. Acta Crystallogr Sect F Struct Biol Cryst Commun 66:1211-7.
22. Marchesini MI, Connolly J, Delpino MV, Baldi PC, Mujer CV, DelVecchio VG, Comerci DJ. 2011. *Brucella abortus* choloylglycine hydrolase affects cell envelope composition and host cell internalization. PLoS One 6:e28480.
23. Connolly JP, Comerci D, Alefantis TG, Walz A, Quan M, Chafin R, Grewal P, Mujer CV, Ugalde RA, DelVecchio VG. 2006. Proteomic analysis of Brucella abortus cell envelope and identification of immunogenic candidate proteins for vaccine development. Proteomics 6:3767-80.
24. Sternon JF, Godessart P, Goncalves de Freitas R, Van der Henst M, Poncin K, Francis N, Willemart K, Christen M, Christen B, Letesson JJ, De Bolle X. 2018. Transposon Sequencing of Brucella abortus Uncovers Essential Genes for Growth In Vitro and Inside Macrophages. Infect Immun 86.
25. Wang Z, Bie P, Cheng J, Lu L, Cui B, Wu Q. 2016. The ABC transporter YejABEF is required for resistance to antimicrobial peptides and the virulence of *Brucella melitensis*. Sci Rep 6:31876.
26. Goolab S, Roth RL, van Heerden H, Crampton MC. 2015. Analyzing the molecular mechanism of lipoprotein localization in *Brucella*. Front Microbiol 6:1189.
27. Sheehan LM, Budnick JA, Blanchard C, Dunman PM, Caswell CC. 2015. A LysR-family transcriptional regulator required for virulence in *Brucella abortus* is highly conserved among the alpha-proteobacteria. Mol Microbiol 98:318-28.
28. Kim HS, Willett JW, Jain-Gupta N, Fiebig A, Crosson S. 2014. The Brucella abortus virulence regulator, LovhK, is a sensor kinase in the general stress response signalling pathway. Mol Microbiol 94:913-25.
29. Silhavy TJ, Kahne D, Walker S. 2010. The bacterial cell envelope. Cold Spring Harb Perspect Biol 2:a000414.
30. Okuda S, Tokuda H. 2011. Lipoprotein sorting in bacteria. Annu Rev Microbiol 65:239-59.
31. LoVullo ED, Wright LF, Isabella V, Huntley JF, Pavelka MS, Jr. 2015. Revisiting the Gram-negative lipoprotein paradigm. J Bacteriol 197:1705-15.
32. Zeytuni N, Zarivach R. 2012. Structural and functional discussion of the tetra-trico-peptide repeat, a protein interaction module. Structure 20:397-405.

33. Cerveny L, Straskova A, Dankova V, Hartlova A, Ceckova M, Staud F, Stulik J. 2013. Tetratricopeptide repeat motifs in the world of bacterial pathogens: role in virulence mechanisms. Infect Immun 81:629-35.
34. Vanderlinde EM, Magnus SA, Tambalo DD, Koval SF, Yost CK. 2011. Mutation of a broadly conserved operon (RL3499-RL3502) from *Rhizobium leguminosarum* biovar viciae causes defects in cell morphology and envelope integrity. J Bacteriol 193:2684-94.
35. Jean NL, Bougault CM, Lodge A, Derouaux A, Callens G, Egan AJ, Ayala I, Lewis RJ, Vollmer W, Simorre JP. 2014. Elongated structure of the outer-membrane activator of peptidoglycan synthesis LpoA: implications for PBP1A stimulation. Structure 22:1047-54.
36. Khan SR, Gaines J, Roop RM, 2nd, Farrand SK. 2008. Broad-host-range expression vectors with tightly regulated promoters and their use to examine the influence of TraR and TraM expression on Ti plasmid quorum sensing. Appl Environ Microbiol 74:5053-62.
37. Wetmore KM, Price MN, Waters RJ, Lamson JS, He J, Hoover CA, Blow MJ, Bristow J, Butland G, Arkin AP, Deutschbauer A. 2015. Rapid quantification of mutant fitness in diverse bacteria by sequencing randomly bar-coded transposons. MBio 6:e00306-15.
38. Willett JW, Herrou J, Briegel A, Rotskoff G, Crosson S. 2015. Structural asymmetry in a conserved signaling system that regulates division, replication, and virulence of an intracellular pathogen. Proc Natl Acad Sci U S A 112:E3709-18.
39. Minor W, Cymborowski M, Otwinowski Z, Chruszcz M. 2006. HKL-3000: the integration of data reduction and structure solution--from diffraction images to an initial model in minutes. Acta Crystallogr D Biol Crystallogr 62:859-66.
40. Emsley P, Cowtan K. 2004. Coot: model-building tools for molecular graphics. Acta Crystallogr D Biol Crystallogr 60:2126-32.
41. Adams PD, Grosse-Kunstleve RW, Hung LW, Ioerger TR, McCoy AJ, Moriarty NW, Read RJ, Sacchettini JC, Sauter NK, Terwilliger TC. 2002. PHENIX: building new software for automated crystallographic structure determination. Acta Crystallogr D Biol Crystallogr 58:1948-54.
42. Murshudov GN, Vagin AA, Dodson EJ. 1997. Refinement of macromolecular structures by the maximum-likelihood method. Acta Crystallogr D Biol Crystallogr 53:240-55.
43. Laskowski RA, Macarthur MW, Moss DS, Thornton JM. 1993. Procheck - a Program to Check the Stereochemical Quality of Protein Structures. Journal of Applied Crystallography 26:283-291.
44. Hagemans D, van Belzen IA, Moran Luengo T, Rudiger SG. 2015. A script to highlight hydrophobicity and charge on protein surfaces. Front Mol Biosci 2:56.
45. Slabinski L, Jaroszewski L, Rychlewski L, Wilson IA, Lesley SA, Godzik A. 2007. XtalPred: a web server for prediction of protein crystallizability. Bioinformatics 23:3403-5.
46. Holm L, Rosenstrom P. 2010. Dali server: conservation mapping in 3D. Nucleic Acids Res 38:W545-9.
47. Williams KP, Sobral BW, Dickerman AW. 2007. A robust species tree for the *alphaproteobacteria*. J Bacteriol 189:4578-86.